Numerical modelling of PCM Melting process embedded in porous media: Effect of heat storage size

Pouyan Talebizadeh Sardari[1,*], Gavin Walker[2], Mark Gillott[3], David Grant[4], Donald Giddings[1]

[1]Fluids and Thermal Engineering Research Group, Faculty of Engineering, University of Nottingham, University Park, Nottingham NG7 2RD, UK

[2]Advanced Materials Division, Energy Technologies Research Institute, University of Nottingham, Innovation Park, Nottingham NG7 2TU, UK

[3]Infrastructure, Geomatics and Architecture Research Division, Faculty of Engineering, University of Nottingham, University Park, Nottingham NG7 2RD, UK

[4]Advanced Materials Research Group, Faculty of Engineering, University of Nottingham, University Park, Nottingham NG7 2RD, UK

Abstract

The aim of this paper is to study the influence of enclosure size in latent heat thermal energy storage (LHTES) systems embedded in a porous medium for domestic usage of LHTES heat exchangers. A 2-D rectangular enclosure is considered as the computational domain to study the heat transfer improvement for a phase change material (PCM) embedded in a copper foam considering a constant heat flux from the bottom surface. Different dimensions of the composite system are examined compared with a system without a porous medium. The thermal non-equilibrium model with enthalpy-porosity method is employed for the effects of

* Corresponding author.

E-mail address: pouyan.talebizadehsardari@nottingham.ac.uk (P. Talebizadeh Sardari).

porous medium and phase change in the governing equations, respectively. The PCM liquid fraction, temperature, velocity, stream lines and the rate of heat transfer are studied. The presence of a porous medium increases the heat transfer significantly, but the improvement in melting performance is strongly related to the system's dimensions. For the dimensions of 200×100 mm (W×H), the melting time of porous-PCM with the porosity of 95% is reduced by 17% compared with PCM only system. For the same storage volume and total amount of thermal energy added, the melting time is lower for the system with a lower height, especially for the PCM only system due to a higher area of the input heat. The non-dimensional analysis results in curve fitting correlations between the liquid fraction and $Fo.Ste.Ra^{-0.02}$ for rectangular LHTES systems for both PCM only and composite PCM systems within the parameter range of $1.16< Ste <37.13$, $0< Fo <1.5$, $2.9\times10^4 < Ra < 9.5\times108$, $0<L_f < 1$ and $0 < Fo.Ste.Ra^{-0.02} < 0.57$. Over a range of system's volume, heat flux and surface area of the input heat flux, the benefit of composite PCM is variable and in some cases is negligible compared with the PCM only system.

Keywords: Phase change material; Porous media; Natural convection; Latent heat thermal energy storage system; Melting process.

Nomenclature

A_m	Mushy zone constant	$\vec{S}$	Source term in momentum equation
A_{sf}	Specific surface area	S_L	Source term in energy equation
C	Inertial coefficient of porous medium	T	Temperature (K)
C_f	Specific heat of PCM (J/kgK)	T_f	Fluid temperature (K)
C_s	Specific heat of porous medium (J/kgK)	T_s	Solid temperature (K)
d_p	Pore size (m)	T_{ref}	Reference temperature (K)
d_l	Ligament diameter of the porous medium (m)	u	velocity components in x-direction (m/s)
$\vec{g}$	Gravitational acceleration (m/s^2)	v	velocity components in y-direction (m/s)

h	Sensible enthalpy (J/kg)		
h_{ref}	Sensible enthalpy at reference temperature (J/kg)	**Greek symbols**	
h_{sf}	Local heat transfer coefficient (W/m^{2}K)	β_f	Thermal expansion coefficient (1/K)
H	Total enthalpy (J/kg)	ε	Porosity
k_e/k_{eff}	Effective thermal conductivity (W/mK)	λ	Liquid fraction
k_f	Thermal conductivity of fluid (PCM) (W/mK)	μ_f	Dynamic viscosity (kg/ms)
k_{fe}	Effective thermal conductivity of fluid (W/mK)	ρ_f	Density (kg/m^3)
k_s	Thermal conductivity of solid (porous material) (W/mK)	$\rho_{f,re}$	Density at reference temperature (kg/m^3)
k_{se}	Effective thermal conductivity of solid (W/mK)	ω	Pore density (PPI)
K	Permeability of porous medium (m^2)	ΔH	Latent heat (J/kg)
L_f	Latent heat of fusion (J/kg)	**Subscripts**	
Re	Reynold number	f	Fluid (PCM)
P	Pressure (Pa)	s	Solid (metal foam)
Pr	Prandtl number	ref	Reference

1. Introduction

LHTES systems are used due to having a high capacity of heat storage, typically 5 to 14 times higher than sensible heat storage systems, with the added advantage of almost constant temperature during the solidification/melting process [1, 2]. LHTES systems have been employed in both domestic and industrial sectors in order to reduce the energy demand [3]. For domestic heat exchangers, LHS can be employed in order to reduce the consumed energy as well as help peak-shaving in the buildings as the main sector of energy consumption [3, 4]. Phase change materials (PCMs) are used in LHTES systems to store heat during the melting process and then release heat during the solidification process. The main challenge of efficient PCM is the long melting time due to low thermal conductivity and low thermal diffusivity within the bulk PCM; these disadvantages lead to limited use of LHTES systems [5]. Methods in the literature that help to overcome the weak characteristics of PCM include the use of a more complex configuration

of heat exchangers [6-9], use of extended metal surfaces [10, 11], use of encapsulated PCM [12-14], use of high conductive nanoparticles [15-18] and the most recent way is the use of a conductive porous medium [19-22].

The use of porous media in LHTES systems enhances the heat transfer rate inside the PCM. Attention has focused on investigating the use of porous media on different heat exchangers to enhance the thermal performance of the system. Py et al. [23], as one of the pioneer researchers, studied a composite paraffin-graphite matrix impregnated by the capillary forces. They presented that the equivalent thermal conductivity of the composite is ranged from 4 to 70 W/mK based on the percentage of paraffin in the matrix instead of 0.24 W/mK for the paraffin. Reducing the porosity of the matrix enhance the thermal conductivity of the composite. They showed a reduction in the solidification time and higher stability of the TES system with a composite structure. Mesalhy et al. [24] performed a numerical analysis on the melting process of PCM embedded in a high conductivity porous matrix using a thermal non-equilibrium model. There is a significant effect of the porous matrix on the rate of heat transfer and melting time. They claimed that although the melting rate increases by using low porosity medium, due to reducing the convection effect, a PCM storage with high porosity and high thermal conductivity is the best technique. Zhao et al. [25, 26] studied on heat transfer enhancement in PCM embedded in a copper metal foam experimentally and numerically. They worked on the effect of porosity and pore density of a metal foam-PCM compared with a PCM only. They showed significant increase of heat conduction rate by using a metal foam. However, in comparison with the PCM only system, the natural convection effect reduces significantly. Lower porosity and higher pore densities can increase the rate of heat transfer in the domain. They showed that the heat transfer increases 5-20 times in the solid phase zone and 3-10 times in the charging process with metal foam compared with the PCM only system, with similar effect during discharge. Tay et al. [27] performed a CFD simulation using ANSYS FLUENT

software accompanied with experimental validation for a complex PCM based heat storage unit. A complicated and unique tubes arrangement for heat transfer fluid were designed to charge and discharge the PCM. They showed the capability of CFD code on simulating phase change in a complex heat storage system. They presented the details of the CFD simulation which can accurately predict the behaviour of LHTES systems. Liu et al. [28] studied using CFD the melting of phase change in a porous medium in a shell and tube LHTES system in 2-D and 3-D cases. They claimed that the melting time can be reduced by more than seven times in comparison with PCM only system. In the study of the pore size, they showed that in general, the pore size has a very small effect on the melting process in the porosity of 95%. For very high pore densities (60 PPI), the natural convection is almost negligible due to high flow resistance in the melting process. Decreasing the pore density (from small sizes such as 10 PPI to the moderate sizes such as 30 PPI), higher performance is achieved due to a higher rate of heat transfer. Sciacovelli et al. [29] performed a CFD simulation on the phase change process in a vertical shell-and-tube LHTES unit. They verified the CFD code using a 2D axisymmetric model with experimental data from the literature. They added copper nanoparticles to the PCM to increase the thermal conductivity and showed that the nano-enhanced PCM with 4% concentration of nanoparticles reduced the melting time by 15% and increase the heat flux rate by 16%. Gupta et al. [30] performed an experimental study and CFD simulation of an active cylindrical LHTES tank for domestic applications compared with water-filled tank due to the high heat capacity of suitable PCMs. They used hydrated salt as the PCM and used OpenFOAM software for CFD simulation. They showed accurate results of the CFD code compared with the experimental data. They reported the advantages of PCM heat storage unit than the water tank in the initial moments; however, the discharging heat was reduced due to the high viscosity of liquid PCM. Therefore, they recommended an improvement in heat exchanger design and the use of heat transfer enhancement methods. Hossain et al. [31] studied a 2D rectangular

enclosure heat storage system using both nanoparticles and porous medium. CuO was considered as the nanoparticles. They considered the source of thermal energy at the upper surface of the enclosure in order to reduce the effect of natural convection in the presence of a porous medium. Nanoparticles increase the thermal conductivity of PCMs and the porous medium increases the rate of heat transfer through the PCM. They showed that the melting process improved more significantly by the presence of porous medium rather than nanoparticles and a faster rate of melting happens at lower porosity and higher volume fraction of nanoparticles. For the porosity of 85%, the melting time reduced from 3100 s for the nanoparticle concentration of 10% to 3440 s without nanoparticles. Zhang et al. [32] studied numerically different metal foams of copper and nickel in a latent heat solar energy storage system using molten salt PCM. They showed the reduced effect of natural convection in the presence of composite metal foam due to the flow resistance. They showed that due to the large difference between the thermal conductivity of metal foam and PCM, a considerable temperature gradient exists between the porous medium and PCM and therefore the thermal non-equilibrium model should be correctly considered in the simulation. They showed the copper metal foam has a better performance than nickel, having the maximum temperature difference of 6.8 °C between the foam and PCM and the reduction in total melting time of 28.3%. Mahdi et al. [33] studied a triplex-tube LHTES system using both Al_2O_3 nanoparticles and copper foam to increase the melting time of the heat exchanger. They showed that simultaneous use of porous medium and nanoparticles can improve the melting of PCM significantly. They showed that by a reduction of PCM volume due to the presence of metal foam and nanoparticles, high porosity metal foam with a low volume fraction of nanoparticles are recommended. By employing 95% porosity copper metal foam, the melting time reduces from 162 minutes for the non-porous case min to 18 minutes; however, employing 5% nanoparticle just reduced the melting time to 130 min.

Based on the presented literature review, researchers employed metal foams to increase the rate of heat transfer in PCM and reduce the melting/solidification time compared with the PCM only systems. However, the benefit of the composite depends on the volume of the PCM which is not mentioned in the literature. Therefore, in this paper, different sizes of the storage system and amounts of heat flux are examined for the copper foam LHTES system compared with the PCM only case to comprehensively study the effect of the porous medium in relation to natural convection in the domain. The thermal non-equilibrium model is employed to model a composite metal foam with PCM in a 2-D rectangular enclosure, representative of domestic thermal storage units, with heat flux from the lower surface. The effect of solid-liquid phase change is considered using the enthalpy-porosity method. The liquid fraction, temperature and velocity distributions, streamlines and melting time are all studied for the composite PCM in comparison with the PCM only in this paper. The results of this paper provide guidelines for the better design of domestic thermal energy storage systems.

2. Mathematical description

In a PCM only LHTES system, heat is transferred to the solid PCM by conduction and then spread out in the liquid PCM by convection and conduction. To increase the heat transfer inside the PCM, a porous foam is prepared and the PCM is injected into the porous media [23]. The heat is more transferred by the high conductivity solid porous medium through the PCM. In the modelling of PCM, to consider the effect of phase change, the enthalpy-porosity technique is used where the porosity is set equal to the liquid fraction in each cell. Then, by applying Darcy's law for fluid flow in the porous medium and employing the Kozeny–Carman equation, the flow is modelled in the mushy zone where the liquid fraction is varied between 0 and 1 [34]. In the presence of a porous medium, in addition to the pressure drop caused by solidified materials, a pressure loss is considered due to viscous and inertial losses in the momentum

equation employing the Brinkman–Forchheimer equation[35]. For simulating heat transfer process in the presence of porous media, two thermal models can be applied i.e. the thermal equilibrium and non-equilibrium models. In the equilibrium model, the liquid PCM and the porous media have the same temperature and the Brinkman–Forchheimer equation is just added to the momentum equation as a new source term (fourth term on the right hand side of equation 2 below) [36]. However, in the thermal non-equilibrium model, the porous medium and fluid are not in thermal equilibrium and the temperatures of the solid and the fluid are solved separately using a semi-heuristic approach based on a local thermal non-equilibrium model. This model is more accurate, and is employed in this study [24, 32] derived first by Vafai and Tien [37] and then modified by Hsu and Cheng [38]. The following assumptions are also assumed in the present numerical investigation [28, 33]:

1. The liquid PCM is considered as an isotropic, incompressible Newtonian fluid.
2. The porous medium is considered open-cell, homogeneous and isotropic.
3. Boussinesq approximation is applied for laminar flow natural convection of the liquid PCM in the momentum equation due to the small temperature gradient in the domain and the flow is considered laminar
4. The volume expansion of the PCM is neglected during phase change.
5. The influence of surface tension on the flow was negligible.
6. All the properties of the PCM are constant.

Based on these assumptions, the set of governing equations for the Brinkman–Forchheimer-extended Darcy model can be formulated as follows [32]:

2.1.Continuity equation:

The Continuity equation is defined as follows based on the mentioned assumptions [35]:

$$\varepsilon \frac{\partial \rho_f}{\partial t} + \nabla . \rho_f \vec{V} = 0 \tag{1}$$

2.2.Momentum equation

The Momentum equations in x and y-directions are given as follows:

- Thermal non-equilibrium model [35]

$$\frac{\rho_f}{\varepsilon}\frac{\partial u}{\partial t} + \frac{\rho_f}{\varepsilon^2}\left(\vec{V}.\nabla u\right) = -\frac{\partial P}{\partial x} + \frac{\mu_f}{\varepsilon}(\nabla^2 u) - A_m \frac{(1-\lambda)^2}{\lambda^3 + 0.001} u - \left(\frac{\mu_f}{K} + \frac{\rho_f C|u|}{\sqrt{K}}\right) u \tag{2-a}$$

$$\frac{\rho_f}{\varepsilon}\frac{\partial v}{\partial t} + \frac{\rho_f}{\varepsilon^2}\left(\vec{V}.\nabla v\right) = -\frac{\partial P}{\partial y} + \frac{\mu_f}{\varepsilon}(\nabla^2 u) - A_m \frac{(1-\lambda)^2}{\lambda^3 + 0.001} v - \left(\frac{\mu_f}{K} + \frac{\rho_f C|v|}{\sqrt{K}}\right) v - \rho_f g \beta \varepsilon \left(T - T_{ref}\right) \tag{2-b}$$

- Thermal equilibrium model [36]:

$$\rho_f \frac{\partial u}{\partial t} + \rho_f\left(\vec{V}.\nabla u\right) = -\frac{\partial P}{\partial x} + \mu_f(\nabla^2 u) - A_m \frac{(1-\lambda)^2}{\lambda^3 + 0.001} u - \left(\frac{\mu_f}{K} + \frac{\rho_f C|u|}{\sqrt{K}}\right) u \tag{3-a}$$

$$\rho_f \frac{\partial v}{\partial t} + \rho_f\left(\vec{V}.\nabla v\right) = -\frac{\partial P}{\partial y} + \mu_f(\nabla^2 u) - A_m \frac{(1-\lambda)^2}{\lambda^3 + 0.001} v - \left(\frac{\mu_f}{K} + \frac{\rho_f C|v|}{\sqrt{K}}\right) v - \rho_f g \beta \varepsilon \left(T - T_{ref}\right) \tag{3-b}$$

On the right side of the momentum equation, the second terms belong to the viscous resistance and the third term is the Kozeny-Carman equation where A_m is assumed equal to 10^5 kg/m^{3}s as recommended in several studies [39-44]. The fourth and fifth terms account for the extension of Darcy's law to explain the non-Darcy effects. Due to the direction of gravitational

acceleration in the negative y-direction, the Boussinesq approximation is added as the sixth term by $\rho_f g\beta\varepsilon(T - T_{ref})$ [33].

Note that the difference between the momentum equations for the non-equilibrium model compared with the equilibrium one is the presences of $(\frac{1}{\varepsilon^2})$ in the first terms on the left and right sides of the equations and also $(\frac{1}{\varepsilon^2})$ in the second term on the left hand side of the momentum equation.

The first term related to the presence of the porous medium is the viscous loss term where K is calculated based on the empirical equation of Calmidi and Mahajan [45] which was obtained from experiments as follows [46]:

$$K = 0.00073{d_p}^2(1-\varepsilon)^{-0.224}\left(\frac{d_l}{d_p}\right)^{-1.11} \quad (4)$$

The second term is an inertial loss term where C is determined as [46]:

$$C = 0.00212(1-\varepsilon)^{-0.132}\left(\frac{d_l}{d_p}\right)^{-1.63} \quad (5)$$

and d_l is the ligament or cell diameter given as [33]:

$$d_l = 1.18 d_p \sqrt{\frac{1-\varepsilon}{3\pi}}\left(\frac{1}{1-e^{-(1-\varepsilon)/0.04}}\right) \quad (6)$$

The characteristics of the porous medium are defined by three parameters including the ε, ω, and d_l and by knowing two of these parameters, the other one can be calculated from Eq. (6) where d_p is given as [33]:

$$d_p = 0.0254(m)/\omega(PPI) \quad (7)$$

Note that PPI means part per inch.

2.3.Energy equation

- Thermal non-equilibrium model

The energy equations for the solid and fluid is given as [35]:

For the PCM:

$$\varepsilon\rho_f\left(C_f + L\frac{d\lambda}{dT_f}\right)\frac{\partial T_f}{\partial t} + \rho_f C_f\left(\vec{V}.\nabla T_f\right) = k_{fe}\nabla^2 T_f - h_{sf}A_{sf}(T_f - T_s) \quad (8\text{-a})$$

For the porous medium:

$$(1-\varepsilon)\rho_s C_s\left(\frac{\partial T_s}{\partial t}\right) = k_{se}\nabla^2 T_s - h_{sf}A_{sf}(T_s - T_f) \quad (8\text{-b})$$

In the energy equation, λ is defined based of the fluid, solidus and liquidus temperatures as [34]:

$$\lambda = \frac{\Delta H}{L} = \begin{cases} 0 & if\ \ T < T_{Solidus} \\ 1 & if\ \ T > T_{Liquidus} \\ \dfrac{T - T_{Solidus}}{T_{Liquidus} - T_{Solidus}} & if\ \ T_{Solidus} < T < T_{Liquidus} \end{cases} \quad (9)$$

and the total enthalpy is the summation of sensible and latent heat given as:

$$H = h + \Delta H \quad (10)$$

where h is defined as:

$$h = h_{ref} + \int_{T_{ref}}^{T} C_p dT \quad (11)$$

and ΔH is the fractional latent heat of the PCM that may vary between zero for solid and L (latent heat of fusion) for liquid.

In the thermal non-equilibrium model, the effective thermal conductivity of the fluid and solid should be determined and employed independently. There are different theoretical models in the literature based on the porous characteristics, the thermal conductivity of solid and fluid [45, 47-50]. The models are classified based on the unit cell. The 'tetrakaidecahedron' cell model of Boomsma and Poulikakos is employed in this study which is first introduced in 2001 [48] and then corrected in 2011 [51]. In this model, the general form of the effective thermal conductivity is defined as follows [48, 51]:

$$k_{eff} = \frac{1}{\sqrt{2}(R_A + R_B + R_C + R_D)} \tag{12}$$

where

$$R_A = \frac{4\sigma}{(2e^2 + \pi\sigma(1-e))k_s + (4 - 2e^2 - \pi\sigma(1-e))k_f} \tag{13-a}$$

$$R_B = \frac{(e-2\sigma)^2}{(e-2\sigma)e^2 k_s + (2e - 4\sigma - (e-2\sigma)e^2)k_f} \tag{13-b}$$

$$R_C = \frac{\sqrt{2} - 2e}{\sqrt{2}\pi\sigma^2 k_s + (2 - \sqrt{2}\pi\sigma^2)k_f} \tag{13-c}$$

$$R_D = \frac{2e}{e^2 k_s + (4 - e^2)k_f} \tag{13-d}$$

where $e = 0.16$ and

$$\sigma = \sqrt{\frac{\sqrt{2}(2 - \left(\frac{3\sqrt{2}}{4}\right)e^3 - 2\varepsilon)}{\pi(3 - 2\sqrt{2}e - e)}} \tag{14}$$

Then, the effective thermal conductivity of fluid and solid are calculated from Eq. (12) as:

$$k_{fe} = k_{eff}|k_{s=0} \tag{15-a}$$

$$k_{se} = k_{eff}\big|k_{f=0} \tag{15-b}$$

Due to lack of an accurate model to describe the local heat transfer between the solid porous medium and the fluid, one simplification is to calculate it based on theoretical studies of other geometries or fitting methods from numerical or experimental results [52-54]. The pores are usually treated as another geometry such as cylinders, spheres or even vertical plate [53,55-57]. All the equations can be found in Ref. [32]. Among different methods, the porous structure is usually considered as cylinders and the laminar flow of liquid PCM in porous structure is considered similar to the flow around a cylinder [16, 28, 32]. Therefore, the laminar fluid flow in the pores is assumed as the flow around a cylinder where the following empirical correlation is used given as [53]:

$$h_{sf} = \begin{cases} 0.76Re_d^{0.4}Pr^{0.37}k_{pcm}/d_l \quad for \quad 0 < Re_d \leq 40 \\ 0.52Re_d^{0.5}Pr^{0.37}k_{pcm}/d_l \quad for \quad 40 < Re_d \leq 1000 \\ 0.26Re_d^{0.6}Pr^{0.37}k_{pcm}/d_l \quad for \quad 1000 < Re_d \leq 20000 \end{cases} \tag{16}$$

where [32]

$$Re_d = \rho_f \sqrt{u^2 + v^2} d_l/(\varepsilon \mu_f) \tag{17}$$

and A_{sf} is given as [16]:

$$A_{sf} = \frac{3\pi d_l (1 - e^{-(1-\varepsilon)/0.04})}{0.59{d_p}^2} \tag{18}$$

- Thermal equilibrium model

The energy equation is given as follows which is the same for the fluid and porous medium [36]:

$$\rho_f \left(C_f + L\frac{d\lambda}{dT_f} \right) \frac{\partial T_f}{\partial t} + \rho_f C_f \left(\vec{V}.\nabla T_f \right) = k_e \nabla^2 T_f \tag{19}$$

where k_e is calculated as the volume average of the thermal conductivities of porous matrix material and PCM given as [28]:

$$k_e = (1 - \varepsilon)k_s + \varepsilon k_f \tag{20}$$

Note that for the PCM only system, in the governing equations, the porosity is equal to 1 and the source terms in the momentum equations due to the presence of the porous medium are omitted.

3. Problem description

The important effect of porous media in LHTES systems is reducing the charging time. Therefore, in this paper, to study the effect of presenting a porous medium, different rectangular geometries with various areas are considered for both porous-PCM and PCM only with various heat fluxes to see the benefits of the system.

3.1.Geometry and Boundary conditions

The schematic of the physical domain studied in this paper is illustrated in Fig. 1. In the system, porous-PCM/PCM only is embedded in a rectangular enclosure with adiabatic walls and a heat flux is implemented at the bottom of the system. Different widths and heights are examined ranging from 12.5 mm to 200 mm to completely investigate the effect of a porous medium in the various geometries using PCM. The material of the container as well as the porous medium is considered to be copper with a thermal conductivity of 387.6 W/m.K. The heat flux is varied from 800 to 6400 W/m^2 regarding the size of the storage system.

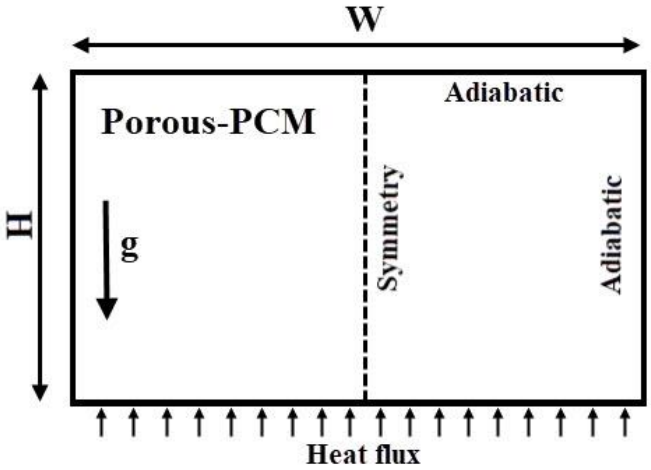

Fig. 1. The schematic of the physical model as well as the boundary conditions

Table 1 lists the studied dimensions of the system in order to study the effects of system width, height, and area. Note that the value of the heat flux is considered various for different simulations which is assigned according to the area of the heat storage system and also the bottom surface.

Table 1. The examined dimension of the heat storage as well as input heat flux

Examined parameters	Width study	Height study	Wall Heat flux (W/mK)

W	50	25	1600
	100		
	200		
	400		
	50	25	6400
	100		3200
	200		1600
	400		800
H	200	12.5	1600
		25	
		50	
		100	
	200	12.5	800
		25	1600
		50	3200
		100	6400
Area	50	100	6400
	100	50	3200
	200	25	1600

RT-58 (RUBITHERM) is considered as the PCM and the physical properties of the RT-58 are listed in Table 2 [28]. The reason for using RT-58 is that the melting point is suitable for domestic usage of LHS units in air and water heat exchangers.

Table 2. Physical properties of RT 58 [28]

Property	RT 58
Liquidus temperature (°C)	48
Solidus temperature (°C)	62
Heat of fusion (kJ/kg)	181
Specific heat (J/kgK)	2100
Density (kg/m^3)	840
Thermal conductivity (W/mK)	0.2
Viscosity (Pas)	0.0269
Thermal expansion coefficient (1/K)	0.00011

Note that PCM is initially at 23 °C to study the solid zone as well as the melting and liquid zones during the heat storage process.

3.2.Numerical modelling

To solve the governing equations, ANSYS-FLUENT software is used in this study with the aid of user-defined functions (UDF) for calculating the interfacial heat transfer coefficient between the fluid and porous medium at each location and each time. The governing equations are discretized using the SIMPLE algorithm with Presto scheme for pressure correction equation and QUICK scheme for the momentum and energy equations. The values for under-relaxation factors are set to 0.3, 0.6, 1 and 0.9 for the pressure, velocity, energy, and liquid fraction, respectively. The convergence criteria for continuity and momentum equations are set to 10^{-6} and 10^{-9} for the energy equation. Note that higher values are also checked for the convergence criteria and no change is seen in the results.

Different density of mesh is studied at the beginning and finally the grid length is considered 1 mm in the x-direction and 0.5 mm in the y-direction due to the existence of natural convection in the y-direction. Therefore, for example, for the dimensions of 100×25 mm, the number of nodes in x and y-direction are 101 and 51, respectively. The mesh density is equivalent to others in the literature in the rectangular geometry [26, 28]. Furthermore, the time step size is considered 0.5s for the porous-PCM and 0.1s for the PCM only. It should be noted that a lower time step size is also studied and the results are almost the same, since the velocity is low and the thermal front movement is similarly low, reflecting a low Peclet number and Courant number situation.

In the Kozeny–Carman equation, A_m is the mushy zone constant usually within the range of 10^4-10^7 kg/m^{3}s which should be determined based on an experimental study and varied with

the geometrical and operational parameters of the system [32]. However, In the presence of a porous medium, due to the small effect of natural convection, A_m has a small effect on PCM behaviour [43]. Figs. 2-a and 2-b illustrate the variation of liquid fraction and mean temperature in terms of time for three different values of Am. As explained and shown, Am has small effects especially during the phase change when the PCM places between the solidus and liquidus temperature. Therefore, the values of 10^5 is considered for A_m in this study.

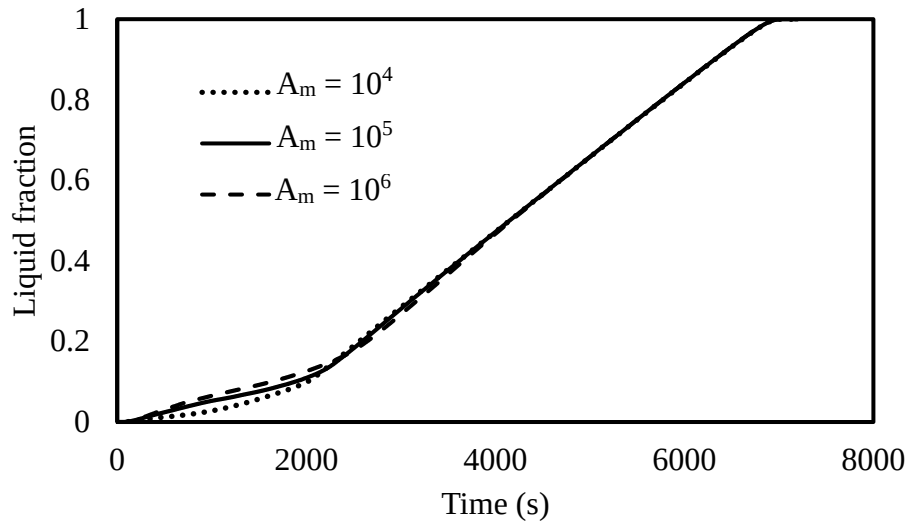

a)

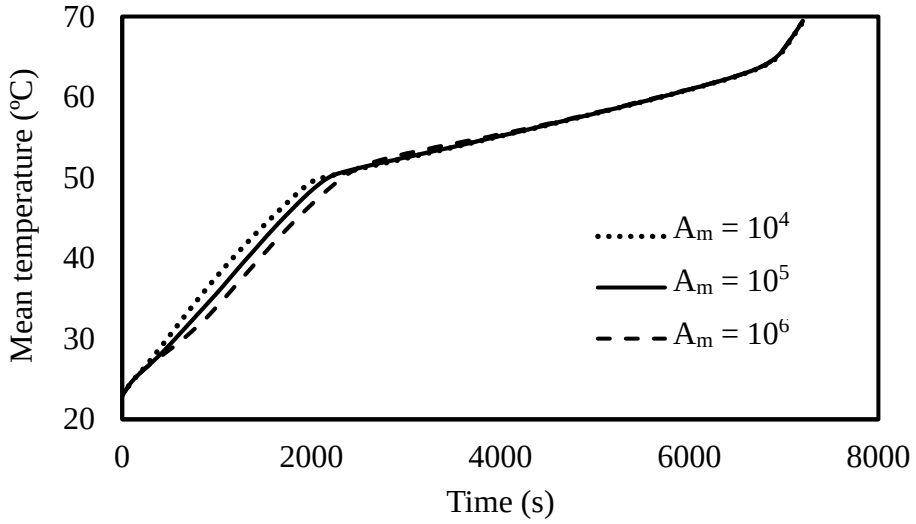

b)

Fig. 2. The variation of a) liquid fraction and b) mean temperature in terms of time for different values of *Am*

4. Model verification

Two different geometries are studied to verify the model for both porous-PCM and PCM only cases in this study. For a porous-PCM, Zhao et al. [25, 26] studied a metal foam PCM with the porosity of 95% and pore density of 10 PPI using RT-58 numerically and experimentally. In Fig. 3-a, the geometry, as well as the boundary conditions, can be seen. Liu et al. [28] also used the data from Zhao et al. [25, 26] to verify their simulations.

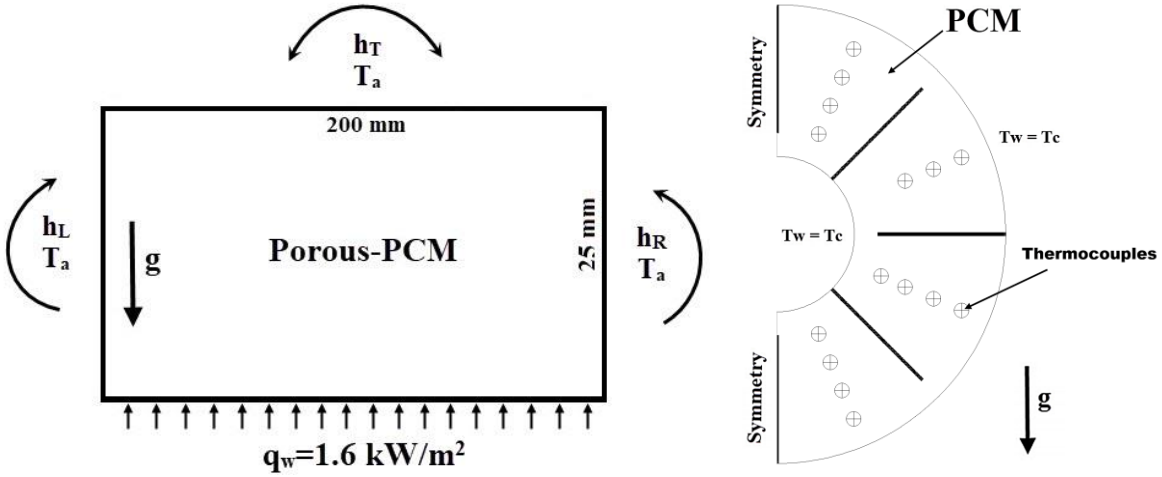

a) b)

Fig. 3. A schematic of the simulated geometry for the model verification for a) Porous-PCM case in 2-D rectangular enclosure and b) A fin-triple tube heat exchanger

The results of the present data in comparison with Zhao et al [25, 26] and Liu et al [28] is displayed in Fig. 4. As shown, an excellent agreement can be found between the non-equilibrium thermal model and the experimental results of Zhao et al. and numerical results of Liu et al. Furthermore, as mentioned in [28], regarding the numerical results of Zhao et al, since a constant

melting temperature is considered in their paper, a small variation was observed with the experimental results. However, in this study and the study of Liu et al. [28], different liquidus and solidus temperatures are considered for the simulations. Note that the temperature at the height of 8mm from the bottom is presented in Fig. 4.

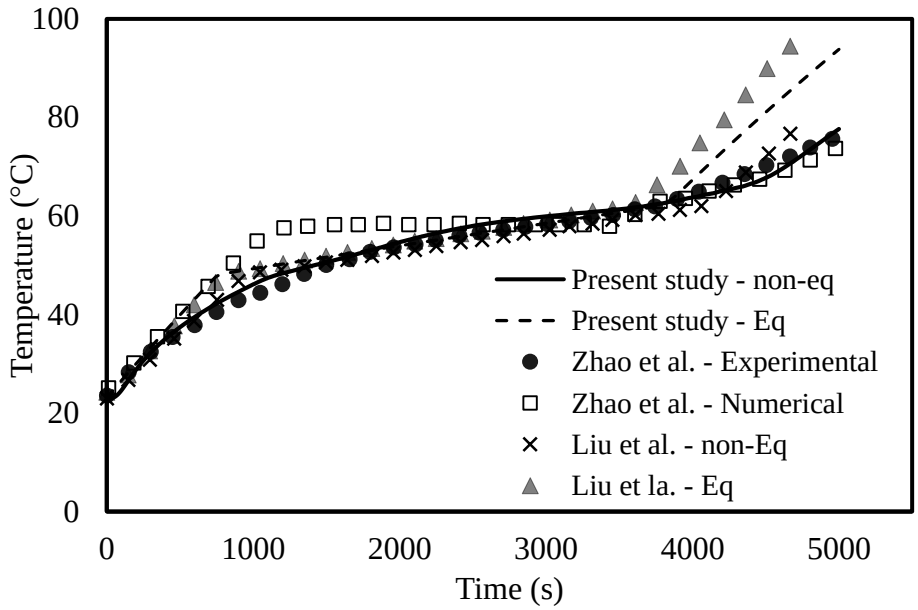

Fig. 4. The verification results of porous-PCM in compare with different numerical and experimental studies in the literature [26, 28]

To verify the code for a PCM only system, the experimental study of Mat et al. [39] is simulated and then the results are compared with each other. In the experiment of Mat et al. [39], a triple tube heat storage system with internal-external fins filled with RT-82 PCM was investigated and the temperature is measured at different locations to find the average temperature of the PCM. In Fig. 3-b, a schematic of the simulated domain is displayed. Fig. 5 shows the results of the current simulation in comparison with the results of Mat et al. [39]. Temperature and liquid fraction are shown in Figs. 5-a and 5-b, respectively. Excellent agreement is achieved in this study in comparison with the experimental and numerical results of Mat et al. [39].

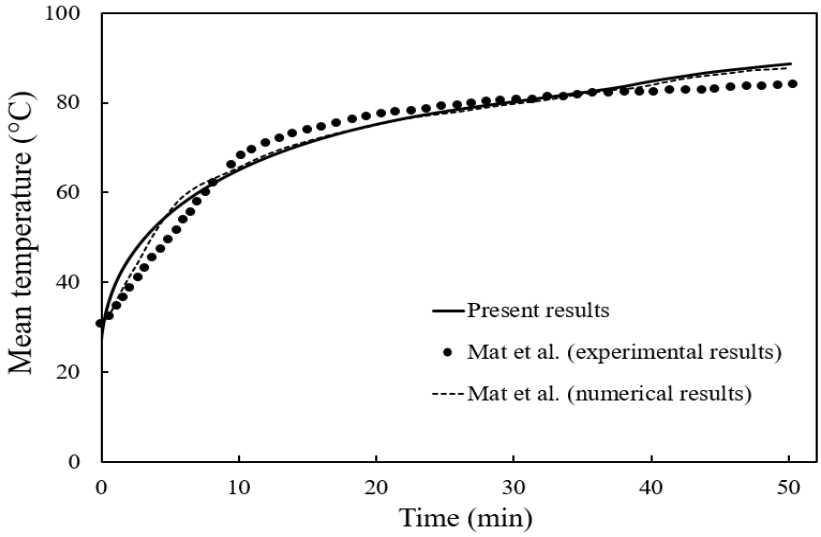

a)

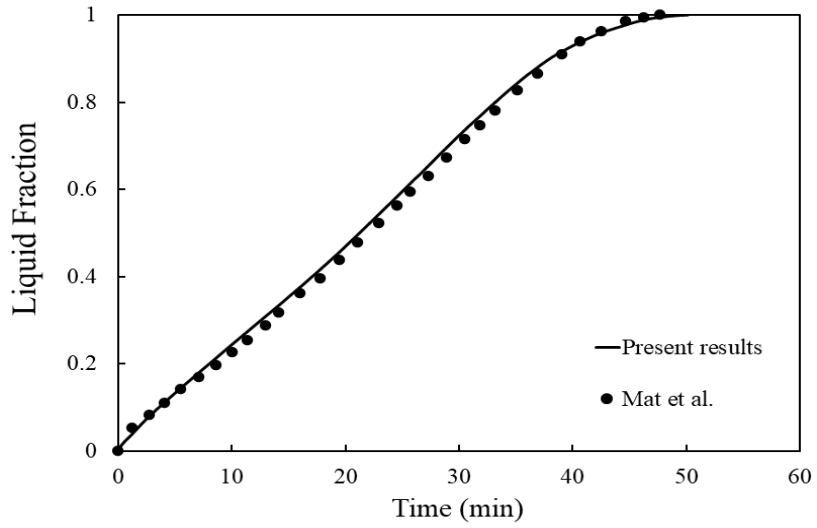

b)

Fig. 5. The verification results for the PCM only system compared with Ref. [39] a) temperature and b) liquid fraction

5. Results and discussion

In the following, first, for the geometry with the dimension of 200×50, the results are presented completely for both porous and non-porous simulations and then the results of other simulations are discussed.

5.1.Effect of porous-PCM compared with PCM only

The presence of the porous medium inside the LHTES system results in the enhancement of heat transfer rate in the domain. Therefore, the heat is moved from the external source faster in the entire domain which can cause a shorter melting time. However, due to making a flow resistance, natural convection also has a small effect on the melting process. The other main advantage of using porous media is that the PCM melts and solidifies more uniformly than the case of PCM only system. In this section, a fundamental discussion is presented by contour plots to better describe the difference between the PCM only and porous-PCM systems.

Fig. 6 shows the contour plot of liquid fraction for the cases of porous-PCM (on the left) and PCM only (on the right) at different times for the dimensions of 200×100 and heat flux of 1600 W/m^2. As shown, at the beginning (before 20 min), both systems melt from the bottom and the liquid is formed. After that, in the porous-PCM, the liquid cannot move properly in the domain due to flow resistance by the solid surface and the heat is transferred by conduction mechanism through the high conductivity metal porous media through the PCM. However, in the PCM only system, natural convection gradually becomes dominant for transferring heat to the top layers and by circulating of a low conductivity PCM and as a result natural convection enhancement, the rate of heat transfer increases. Therefore, at the time of 40 minutes, PCM is melted more in the PCM only system rather than composite PCM system. Another issue is that, as can be seen easily after the time of 60 minutes, since the heat is transferred to the top layer by the porous medium very quickly, the top layers of the PCM melt at almost the same time similar to the bottom layers, however, with a lower melting rate. However, for the PCM only case, it can be seen that the top layers are solid until the moving interface of liquid-solid region rises to the top layers. This a big advantage of porous PCM system especially in discharge time when the entire PCM solidifies almost at the same time.

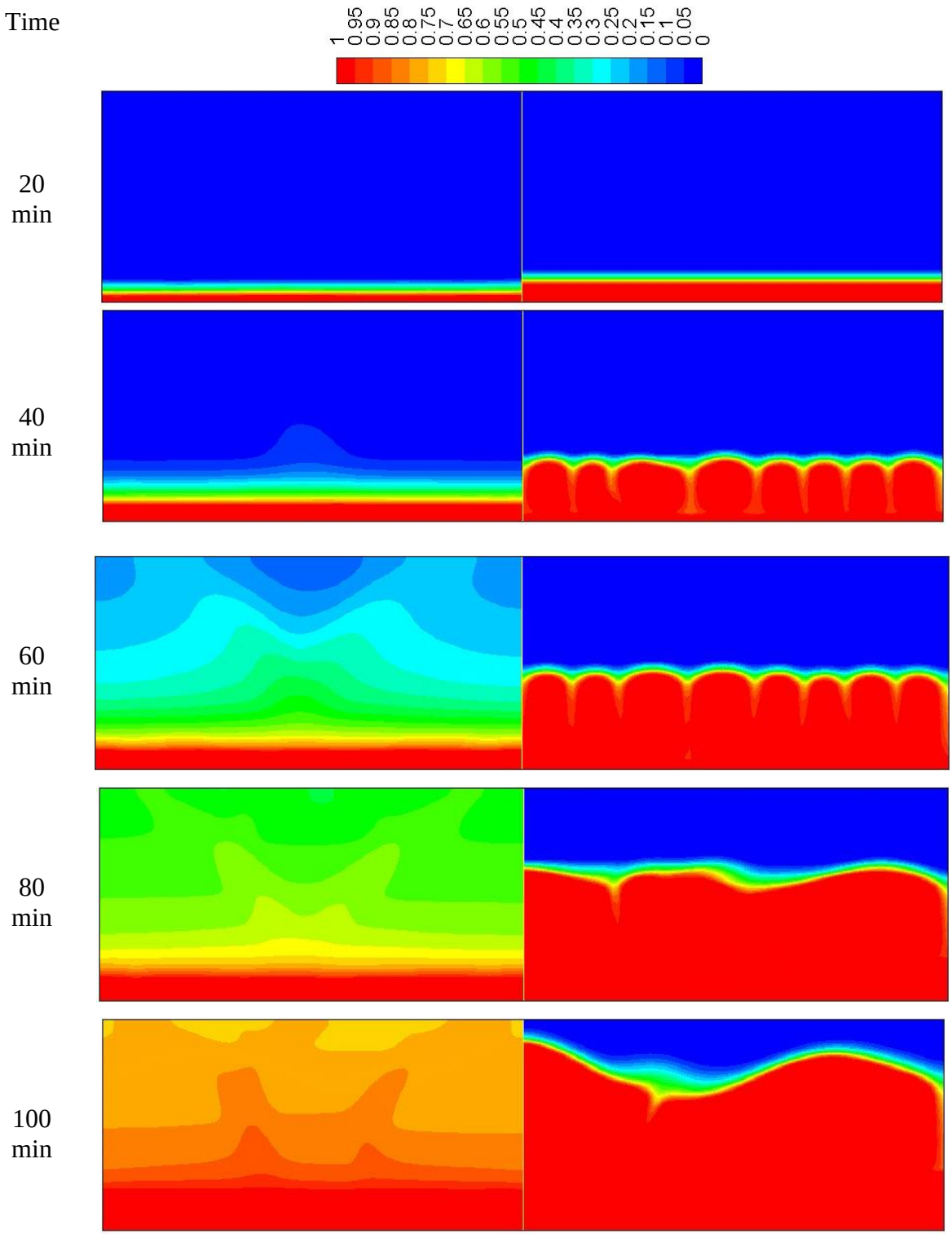
Time
1
0.95
0.9
0.85
0.8
0.75
0.7
0.65
0.6
0.55
0.5
0.45
0.4
0.35
0.3
0.25
0.2
0.15
0.1
0.05
0
20 min
40 min
60 min
80 min
100 min

120 min

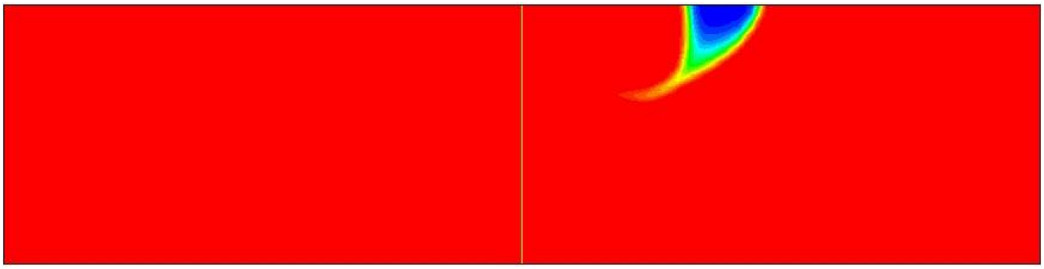

Fig. 6. The Liquid fraction at different time for the PCM only system (on the right) and porous PCM system (on the left)

Fig. 7 shows the contour plot of temperature at the times of 40, 80, and 120 minutes for the systems of porous-PCM (on the left) and PCM only (on the right). As shown at the time of 40, due to absorbing heat by the porous medium and transferring it to the top layers due to a higher conductivity, the heat is transferred faster to the top and higher temperature can be found at the top layers. However, for the PCM only case, the temperature is at the initial temperature at the top layers. Furthermore, since the natural convection dominates, the Benard formation can be seen in the domain. However, for the porous-PCM, just the conduction heat transfer can be seen. As time passes, natural convection starts affecting the porous-PCM to a very small extent which is the reason for a higher temperature in a circulating shape in the presence of porous-PCM. However, for the PCM only system, the generated vortices due to natural convection start joining together and forming bigger vortices as can be seen at the time of 80 minutes. This is established in the literature [58]. Furthermore, in the entire system during the melting process, a lower temperature gradient happens in the presence of porous medium; the magnitude of maximum temperature is less than that for the PCM only case; the magnitude of minimum temperature is much higher than PCM only. For example, the maximum and minimum temperatures are 357 K and 327 K for the porous-PCM case and 372 K and 311 K for the PCM only case, at 80 minutes. Note that the variation of the temperature of porous medium is very small in the entire domain and changes from 329.9 K to 332.2 K. It means that the maximum

temperature difference between the liquid PCM and porous medium is 40 K. It shows the necessity of using the non-equilibrium thermal model on tackling porous-PCM. At the time of 120 min, when the porous PCM melts completely and the PCM only system is still in melting process, again, a low temperature gradient is seen in the porous-PCM and a high temperature gradient in the PCM only case.

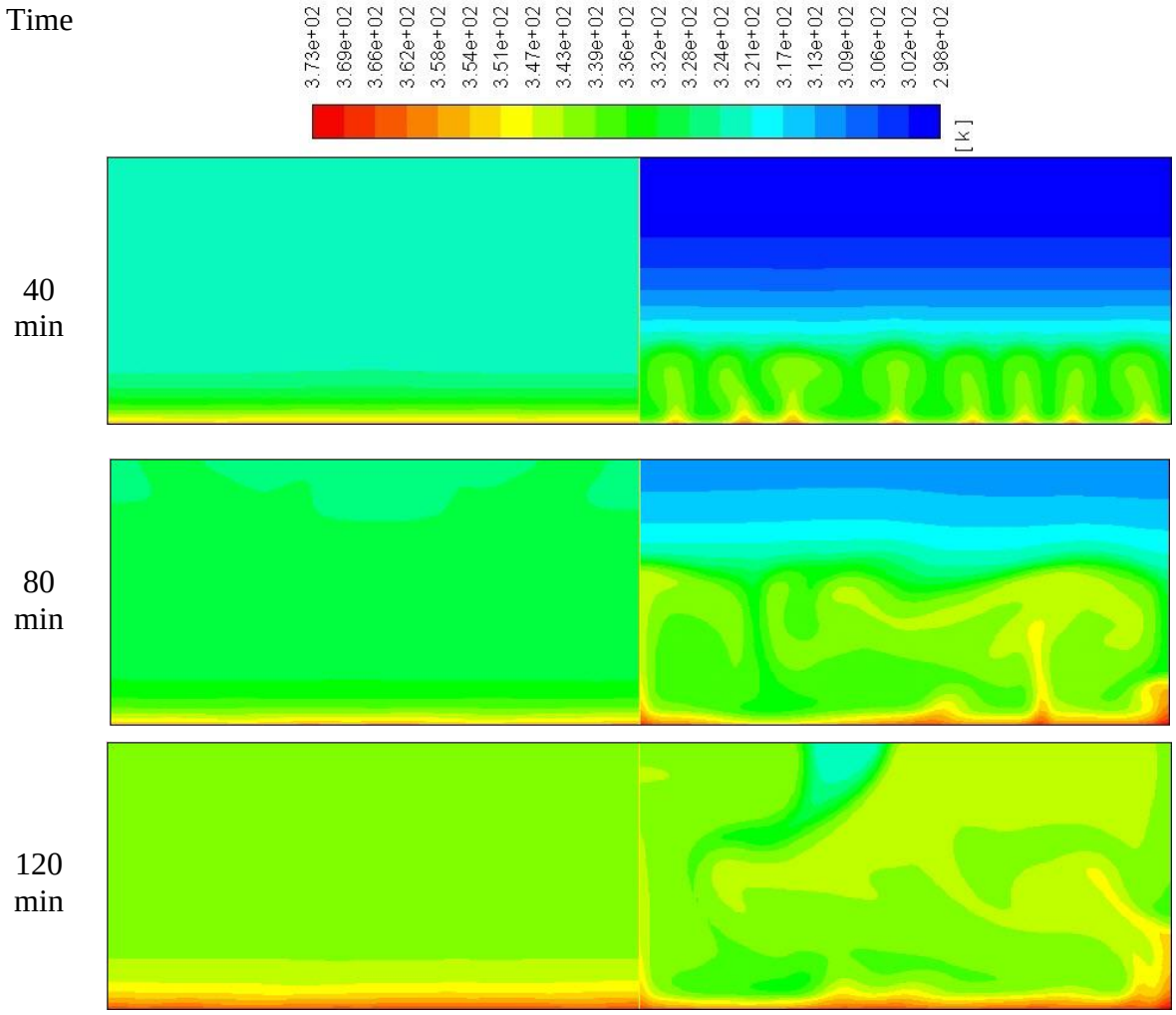

Fig. 7. The temperature distribution at different time for the systems of PCM only (on the right) and porous PCM (on the left)

To show the effect of natural convection in the domain, Fig. 8 displays the velocity contours as well as the streamlines for both systems of porous PCM and PCM only at different times of

40, 80 and 120 minutes. In the presence of porous media, the effect of natural convection is much lower which is well established in the literature [26]. However, in a porous-PCM, when a noticeable amount of liquid is made in the domain and the temperature rises significantly, natural convection affects the distribution of temperature. At the beginning, several vortices are generated in the small melted area and the Benard formation can be seen in natural convection. Then, as time passes and the melting area increases, the vortices merge together and create a bigger recirculation area [58]. Furthermore, the magnitude of velocity is lower by three orders of magnitude for the porous-PCM than the PCM only, which proves the small effect of natural convection in the presence of porous media. However, for the PCM only system, the main mechanism of heat transfer is natural convection, which causes higher values of velocity magnitude in the domain. The average velocity magnitude inside the PCM is 2.8×10^{-7} m/s for the porous-PCM and 2.9×10^{-4} m/s for the PCM only at 80 minutes.

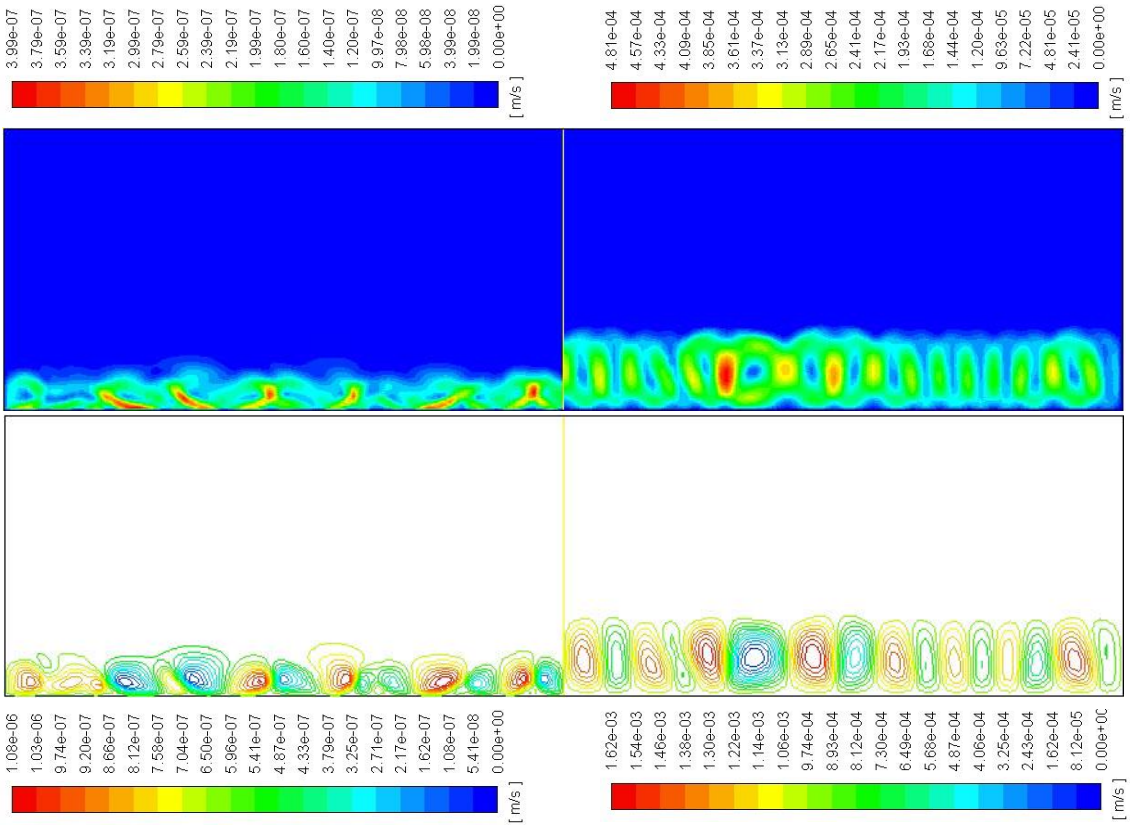

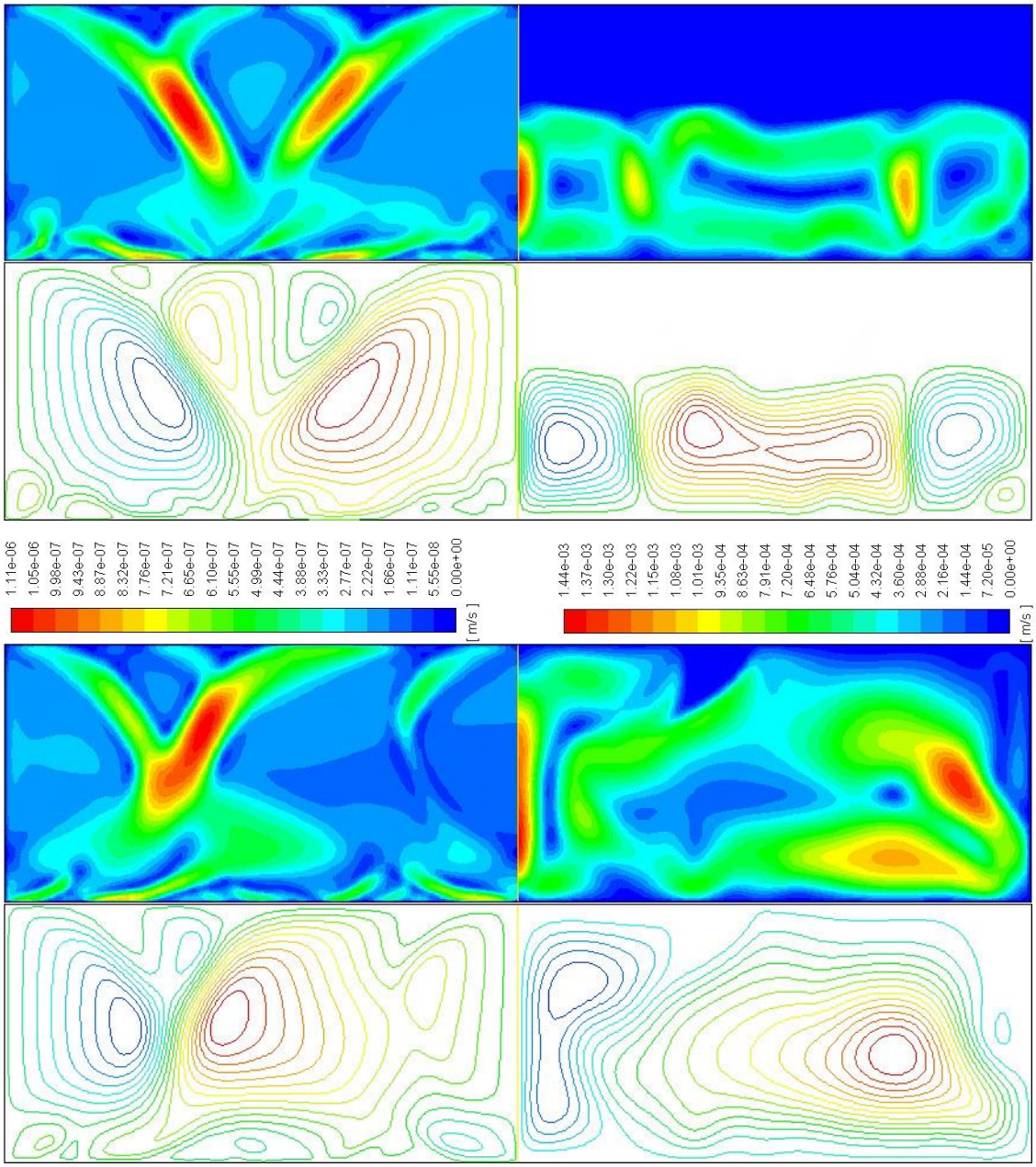

Fig. 8. a) The velocity contours and b) the streamlines for porous-PCM (on the left) and PCM only system (on the right) at the different times of 40, 80 and 120 minutes

Fig. 9 displays the average temperature of the porous medium, the PCM embedded in the porous medium and the PCM only system as a function of time. As shown, the porous medium temperature is higher than the PCM temperature in the composite PCM foam until the time of almost 40 minutes and then the temperatures are almost equal. Furthermore, the temperature of PCM in the presence of porous medium is higher than PCM only system until the time of

40min due to a higher rate of heat transfer through the metal foam. After that, as shown in the contours of temperature, the temperature in the PCM only system is higher than the porous-PCM. At last, after the entire PCM is melted. The temperature rises and is equal for both cases of the porous-PCM and PCM only.

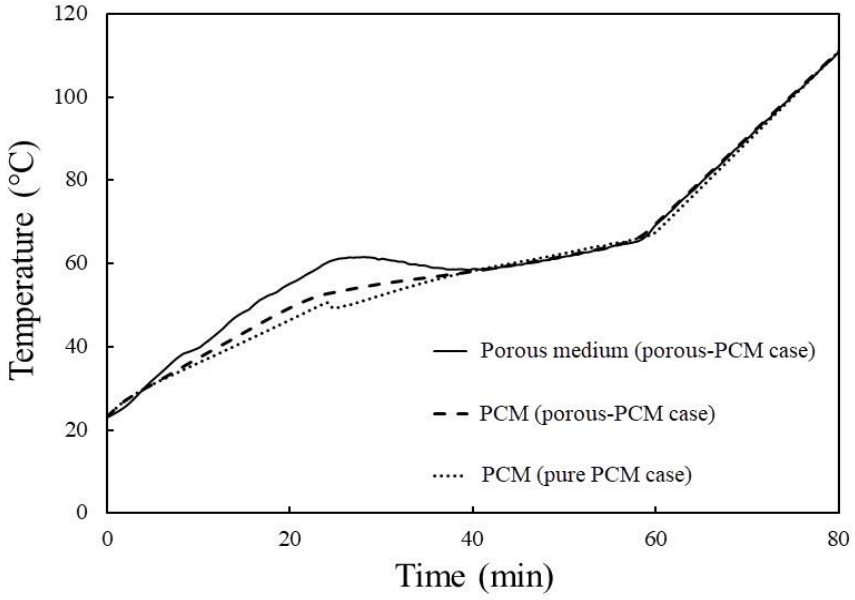

Fig. 9. The variation of mean temperature of porous media and porous-PCM in comparison with the PCM only system

Fig. 10 presents the average temperature at different locations for both systems of PCM only and porous-PCM. For the PCM only system, the difference between the temperatures of different lines are high since enough time is needed that the heat is transferred to the top layers. For the mean temperature of the first line (Y=12.5 mm), at almost time of 40 minutes, the PCM starts melting at the temperature of 48 °C. However, for the middle line (Y=25 mm), almost after 70 minutes, the PCM starts melting. Furthermore, for the porous PCM, due to a high rate of heat transfer, the temperatures of the lines are too close to each other and for all of them, the PCM starts melting almost from the time of 40 minutes until the time of around 120 minutes

from the beginning. For PCM only system, the wall temperature increases with a high rate and then decreases sharply at about 20 minutes. This can also be seen for the porous-PCM case, but with only a small reduction. The reason is that at the melting point, PCM absorbs the heat from the bottom wall. By natural convection and recirculation of the flow for each of the generated vortices, cooler fluid moves to the bottom layers which absorbs more heat from the bottom and therefore causes a temperature reduction on the surface. Note that the melting point of PCM is a lot lower than the temperature of the bottom plate especially in the case of PCM only. This issue can be seen in the literature in cases of heat flux boundary condition [25, 59].

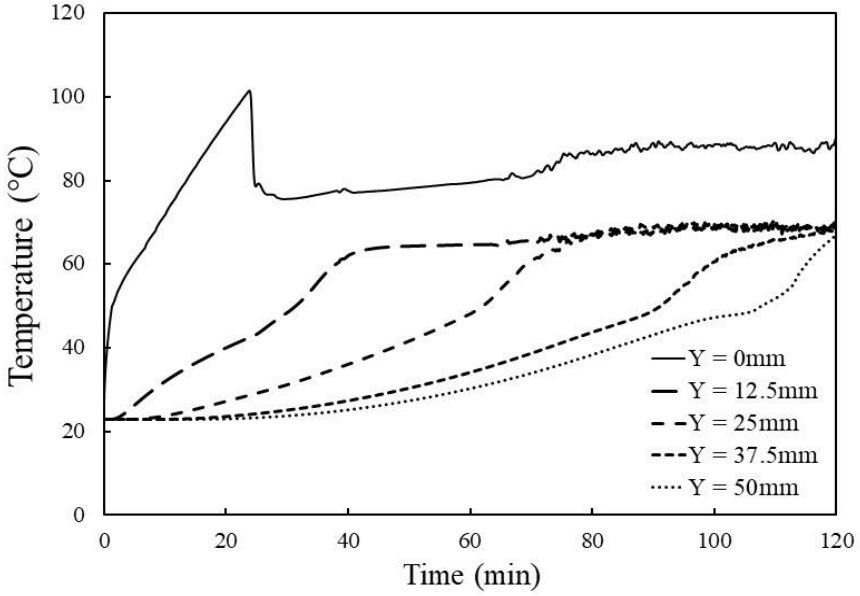

a)

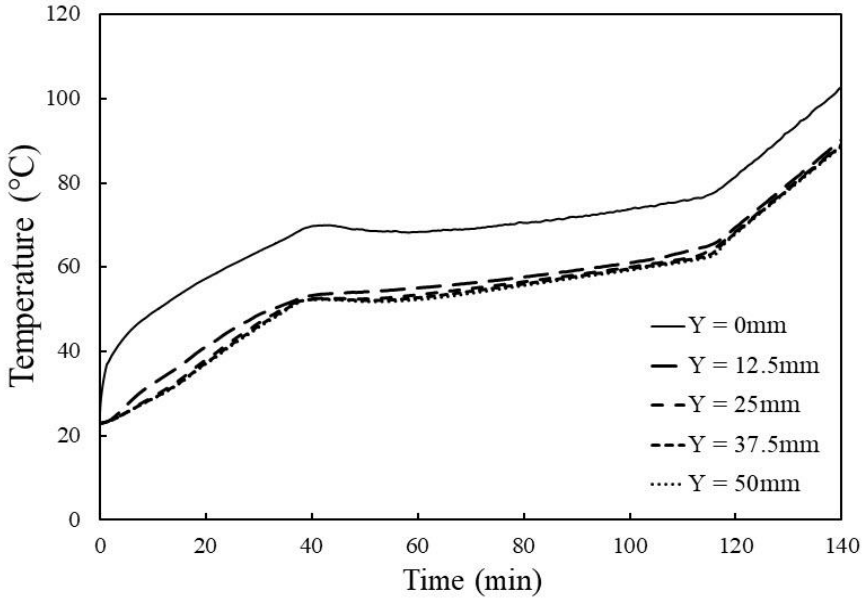

b)

Fig. 10. The mean temperatures of different vertical locations for a) PCM only system and b) porous PCM system

Figs. 11-a and 11-b display the mean temperature difference between the bottom wall and half height position (midline) as a function of time and half height position temperature, respectively, to show the enhancement of heat transfer rate for the porous-PCM over the PCM only system. In the solid zone, especially, and also the liquid zone, significant heat transfer enhancement occur in the presence of the porous medium as indicate by low ΔT. Note that a reduction of temperature difference occur due to the enhancement of natural convection for the PCM only system [25]. Regarding the average temperatures in different phase zones (Fig. 11-b), it can be seen that the overall thermal diffusivity in the case of the porous medium is almost 2.5 times in the solid zone and 1.8 times in the mushy zone and 1.5 times in the liquid zone which is varied for different dimensions of the system. Note that in Fig. 11-b, the mean temperatures at each phase zones are showed by colour lines for porous-PCM and PCM only cases.

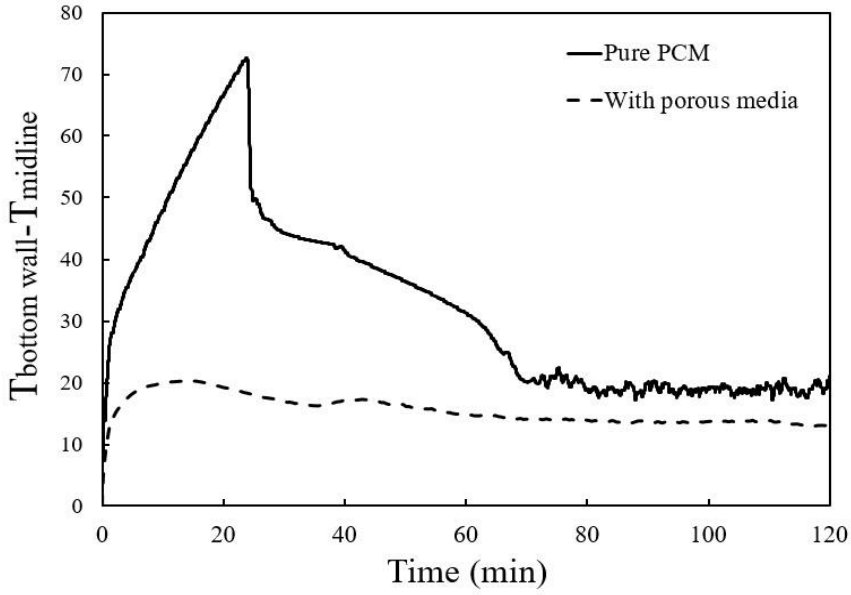

a)

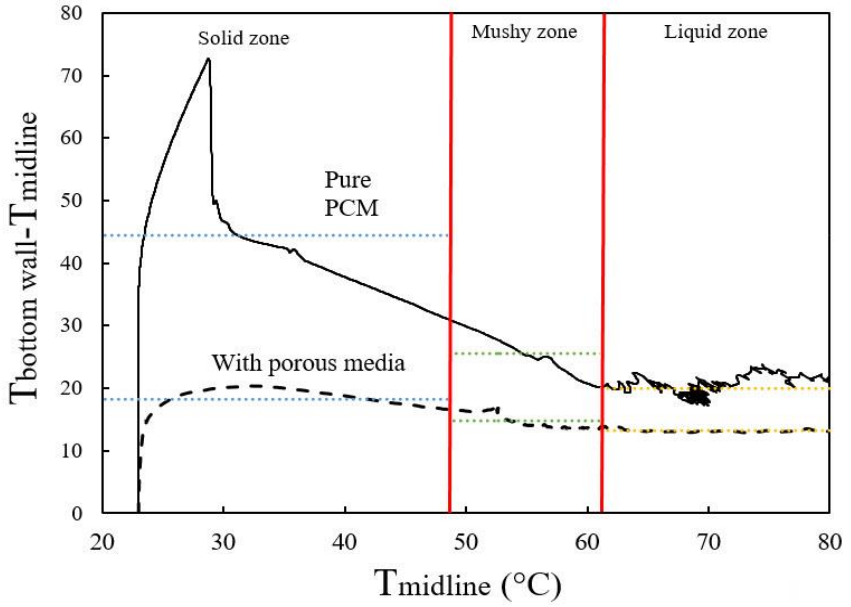

b)

Fig. 11. The temperature difference between the bottom wall and the mid-wall as a function of a) time and b) mid wall temperature

A comparison of the liquid fraction for both studied cases is shown in Fig. 12. As shown, at the beginning, the liquid fraction of PCM only system is a little higher than the porous-PCM. The reason is that the porous medium transfers the induced heat flux to the top layers and the PCM does not receive most of the heat for melting in comparison with the PCM only system.

In other words, there isn't a build-up of heat in the lower levels as the heat is more effectively transferred to the top level by the porous medium. Hence, it takes longer for the lower levels to reach the melting point. Without the porous medium, the heat is trapped in the lower levels and hence the PCM in the lower levels reach the melting point quicker.

After that, the rate of melting increases when the heat is transferred to the entire domain and the entire PCM starts melting. The melting time is higher for the PCM only system, as expected, but the difference between the systems of porous-PCM and PCM only in the melting is not too significant due to the small dimensions of the system and as a result small meting times are observed.

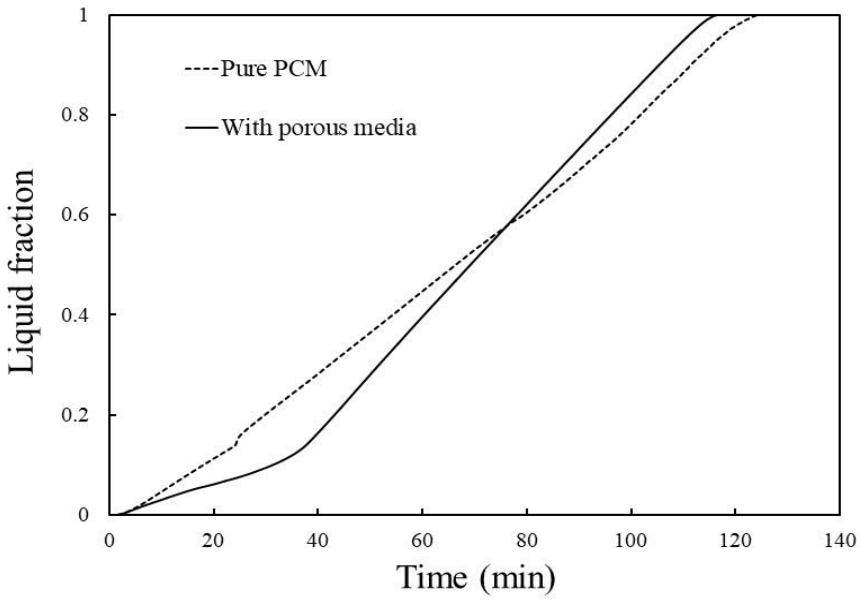

Fig. 12. The mean liquid fraction at different time for both PCM only and porous-PCM cases

5.2.Effect of heat storage height

By increasing the height of heat storage system with constant heat flux of 1.6 kW/m^2 from the bottom, the melting time increases. However, in the porous-PCM system, due to the presence of high conductivity porous medium, the heat is transferred faster to the top layers and

therefore, the presence of porous medium is more effective. Fig. 13 displays the variation of the liquid fraction as a function of time for different heights of the storage system. As shown, by doubling the height and therefore volume of the system, double melting time almost occurs i.e. the rate of heat transfer enhancement is almost constant in porous-PCM systems.

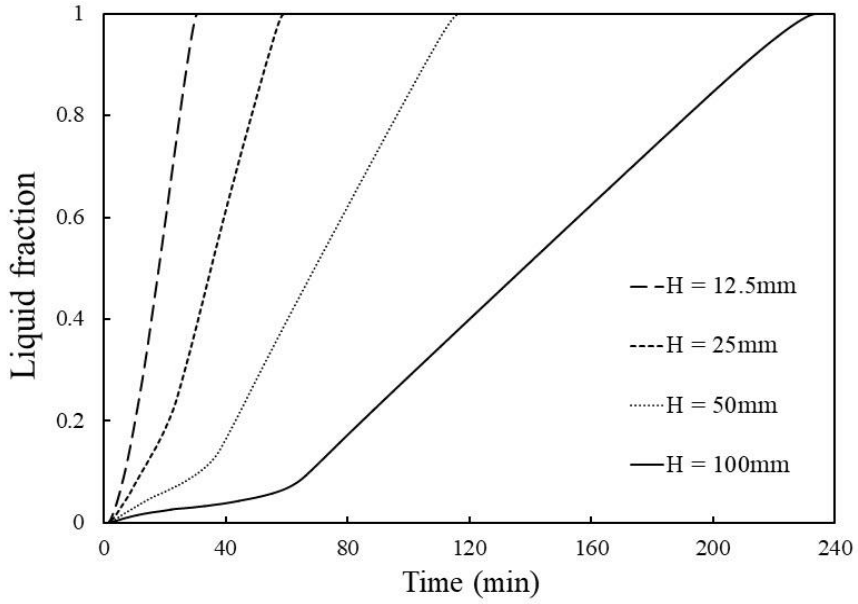

Fig. 13. Mean liquid fraction at different time for porous-PCM for various heights of the storage system

Fig. 14 shows the melting time for different heights for the constant heat flux for the porous-PCM in comparison with the PCM only system. As shown, by increasing the height of the heat storage system, the melting time increases at almost constant rate. Furthermore, the rate of enhancement in the melting time is higher for the PCM only system due to lack of porous medium with the produced free convection. However, the melting time for the storage system with the height of 12.5 mm for the PCM only system is almost equal to the porous-PCM. After that, the difference of melting time between the PCM only system and porous-PCM increases for higher heights of the storage system. Note that for very small heights, the PCM melts from the bottom entirely and the presence of porous medium has no effect on the melting time. In

other words, before that the porous medium is able to affect the PCM, all the PCM melts and therefore the presence of porous medium has no effect.

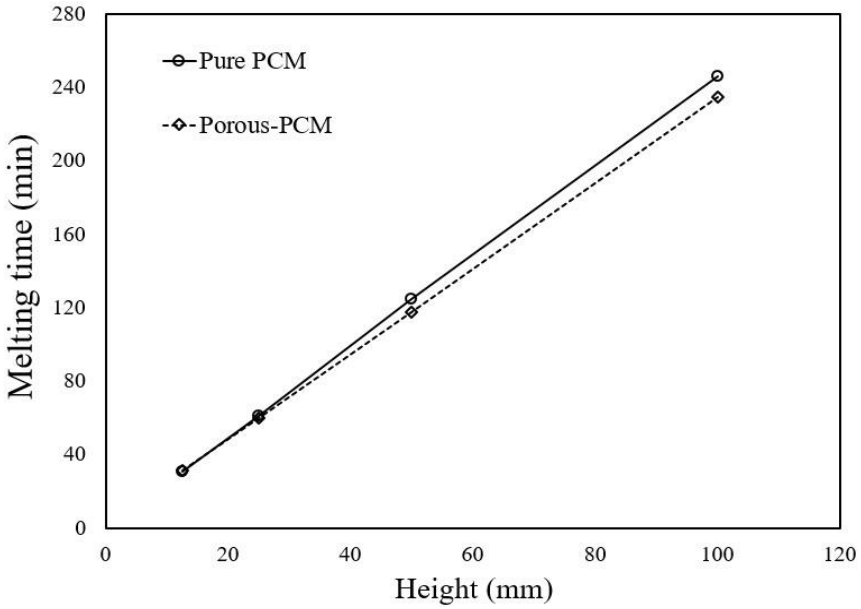

Fig. 14. The effect of system height on the melting time for a constant induced heat flux for both systems of PCM only and porous-PCM

Fig. 15 illustrates the melting time of both porous PCM and PCM only cases considering different heat flux from the bottom according to Table 1. The heat flux is increased according to the increased volume of the system. As shown, for the porous-PCM, due to increasing the rate of heat transfer by increasing the surface area of the system boundaries, the melting time is almost equal for different heights of the storage system. Just for the height of 100 mm, a little increase in the melting time can be seen due to the large size of the storage system. However, for the PCM only system, the melting time increases with increasing the height with much higher rate than the porous-PCM.

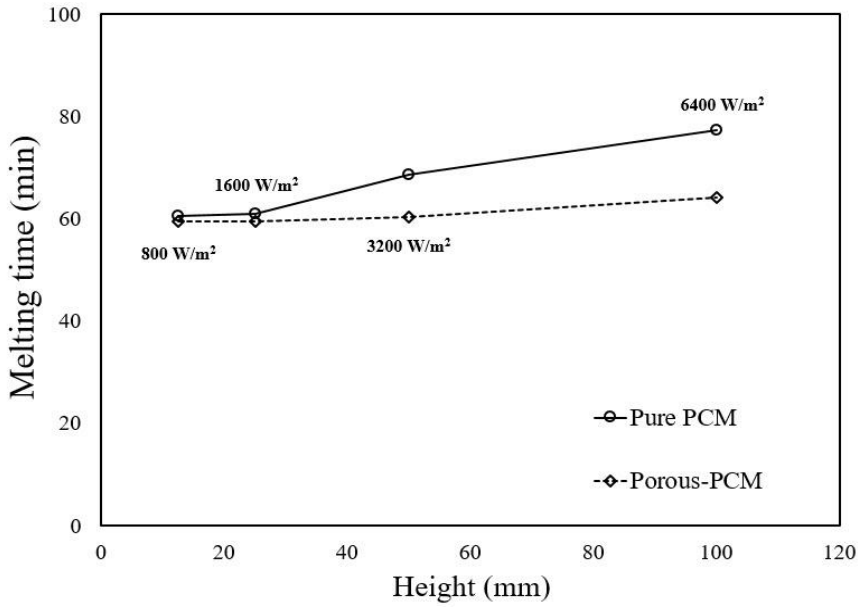

Fig. 15. The effect of system height on the melting time for various induced heat flux regarding Table 1 for both cases of PCM only and porous-PCM

5.3.Effect of heat storage width

By increasing the width of the storage system for a constant height, if a constant heat flux is induced to the bottom wall, it is obvious that the melting time is almost constant. Therefore, to better understand the effect of heat storage width, the storage systems with various widths and heat fluxes are examined regarding Table 1. Fig. 16 displays the variation of the liquid fraction for different widths and heat fluxes of the storage system. As shown, similar to the height study, due to the presence of the porous medium, the melting time almost increases in a constant rate.

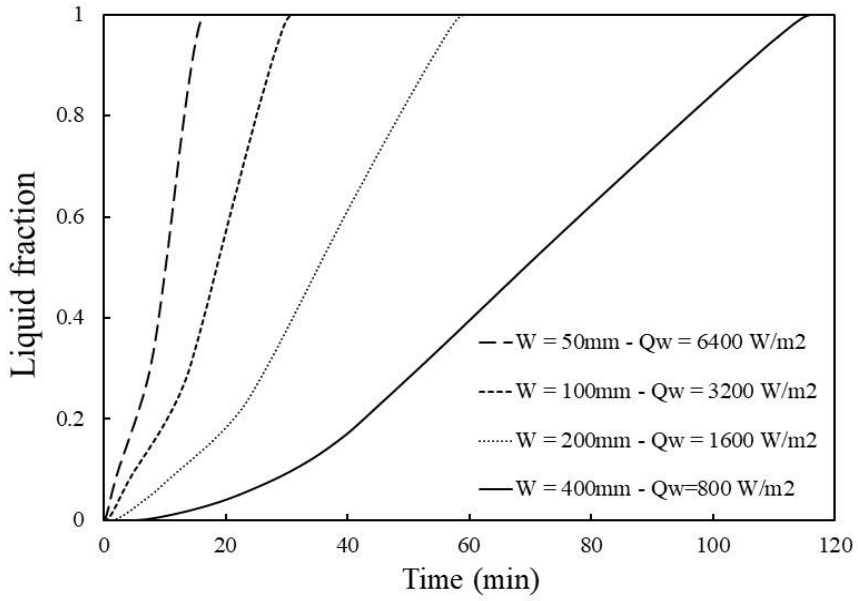

Fig. 16. The mean liquid fraction at different time for porous-PCM for different systems with various widths and heat fluxes

Figs. 17-a and 17-b display the variation of melting time for both cases of PCM only and porous-PCM for constant and variable induced heat fluxes according to Table 2 from the bottom, respectively. As mentioned, for a constant heat flux, the melting times for different widths of the storage system are almost constant for both cases of PCM only and porous-PCM. Just for the PCM only system, the melting time is a little higher than that for the porous-PCM. As shown in Fig. 17-b, by applying different heat fluxes proportional to the system's width, the melting time increases with a constant rate for both systems of PCM only and porous-PCM. In contrast to the height study, the same increment can be seen between the melting time of PCM only system and porous PCM system similar to the constant heat flux.

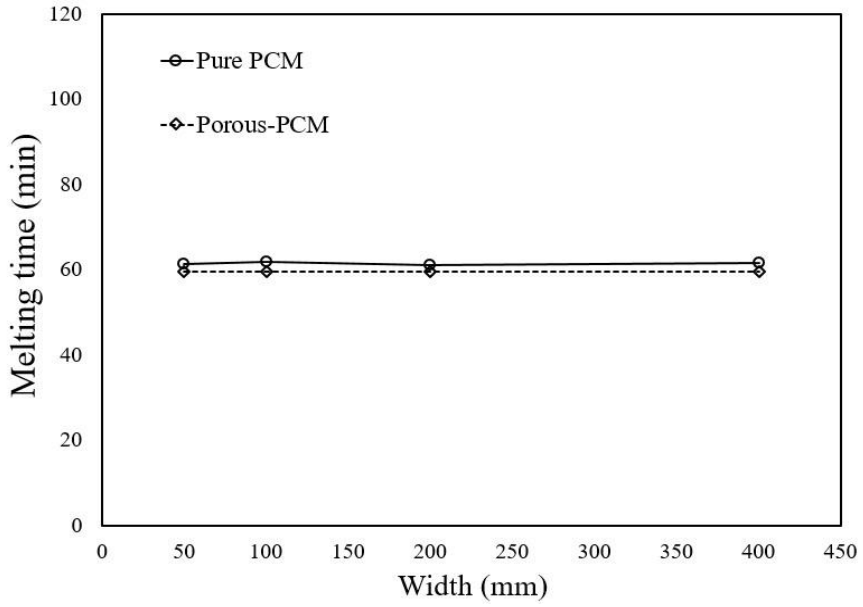

a)

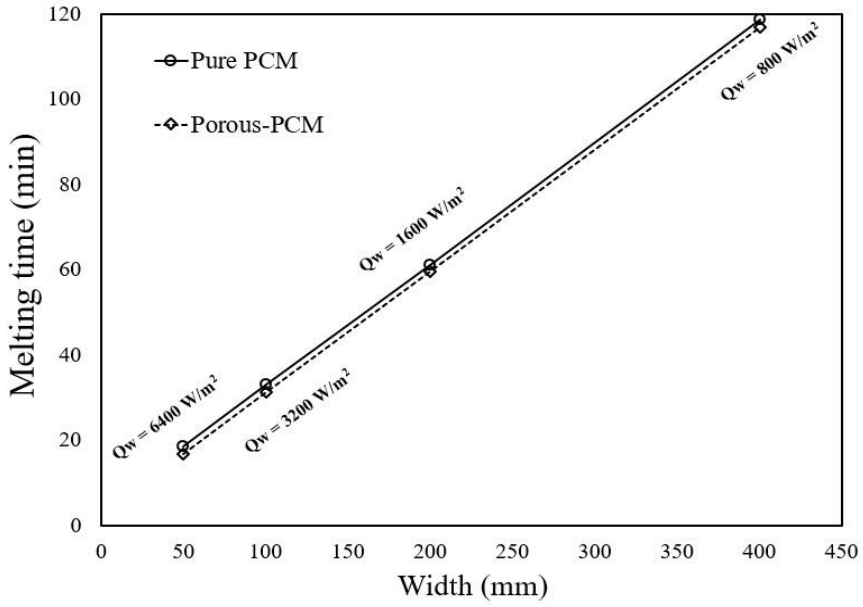

b)

Fig. 17. The effect of system width on the melting time for a) a constant induced heat flux and b) different heat fluxes regarding Table 1 for both cases of PCM only and porous-PCM

5.4.Effect of the heat storage dimensions

To study the effect of constant surface area of the system, three different geometries, with the dimensions of 200×25, 100×50 and 50×100 are studied according to Table 1. Since the amount of input heat should be equal for better comparing the systems, the heat flux is changed for

them related to the bottom surface which is equal to 1600, 3200 and 6400 W/m^2, respectively, for more rate of heat input.

Fig. 18 shows the variation of the liquid fraction for three studied heat storage sizes with the same area through the time. As shown, due to the presence of porous medium and enhancement of heat transfer rate inside the domain, the difference on the melting time is small between the studied geometries. Just in the case of 50×100 due to a large height of the system which causes a larger time to transfer heat from the bottom to the entire area even at much higher heat fluxes. Therefore, it can be concluded that even in the presence of porous medium in LHTES systems, by considering the heat source from the bottom, a system with a lower height has a shorter melting time and therefore is recommended.

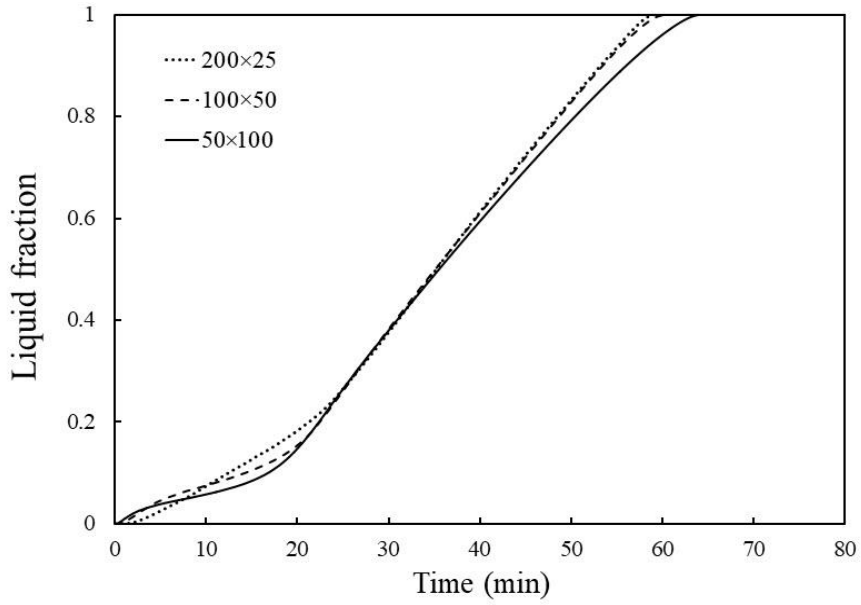

Fig. 18. The mean liquid fraction at different time for porous-PCM for different dimensions of the storage system with the same area

Fig. 19 displays the total melting time for the systems with and without considering the porous medium for different dimensions of the LHTES systems with the same area. As shown, the

effect of heat storage dimensions is more pronounced when a PCM only system is used in the system. It has a small effect when a porous PCM is employed.

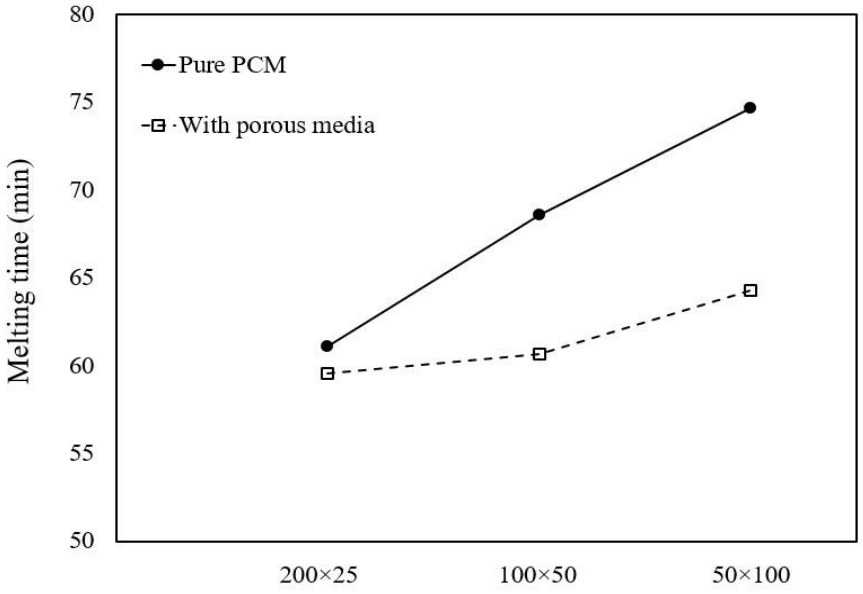

Fig. 19. Effect of system area on the melting time of both cases of PCM only and porous PCM LHTES system

5.5.Dimensionless analysis

To generalize the effect of different parameters, a non-dimensional analysis is performed to normalize the liquid fraction. The first non-dimensional number utilized in unsteady heat transfer problems is Fourier number given as [36]:

$$Fo = \frac{\alpha t}{H^2} \tag{21}$$

where α is the thermal diffusivity (m^2/s), t is time from the start point of the melting and H is unit height.

Stefan number is employed in latent heat storage problems as the ratio of sensible to the latent heat given as:

$$Ste = \frac{C_p \Delta \mathrm{T}}{L} \tag{22}$$

where [60]

$$\Delta \mathrm{T} = \frac{q_w H}{k} \tag{23}$$

Therefore, Stefan number is defined as [60]:

$$Ste = \frac{C_p q_w \mathrm{H}}{kL} \tag{24}$$

For natural convection problems, Grashof number or more comprehensively Rayleigh number is used indicating the ratio of natural convection to conduction heat transfer and for a uniform wall heating flux is defined as [61]:

$$Ra = \frac{\rho^2 g \beta C_p q_w \mathrm{H}^4}{k^2 \mu} \tag{25}$$

The mentioned dimensionless parameters are employed in different studies in the literature for defining the variation of liquid fraction [42, 60-64]. To find the variation of liquid fraction with the mentioned dimensionless parameters, due to having a transient problem, the effect of Fourier number is studied. Based on the literature and due to the fact that the liquid fraction is directly a function of time, it is proposed that the liquid fraction is varied with the Fourier number directly. Fig. 20 illustrates the variation of liquid fraction in term of Fourier number for different Stefan number for PCM only system. Note that for different simulations, Stefan number is calculated based on the dimensions and heat flux and also properties of the PCM according to Eq. (24). For a constant Stefan number, the variation of liquid fraction is almost similar for different cases (Shown for the Ste=2.32 and Ste=9.28). However, as shown, liquid fraction is varied by changing the Stefan number and therefore the Fourier number alone is not sufficient to generalize the liquid fraction due to the effect of latent heat and phase change. As shown, a higher liquid fraction is achieved by reducing the Stefan number at a constant Fourier number or a constant liquid fraction is achieved at a higher Fourier number for a lower Stefan

number which is also reported in the literature [61]. The reason can be explained based on Eq. (24). For constant properties of PCM and a constant height, Stefan number decreases by increasing q_w and therefore, at a same time or for equal furious numbers, a higher liquid fraction is achieved. Fig. 20-b illustrates the variation of liquid fraction for different porous cases showing a similar trend with non-porous cases.

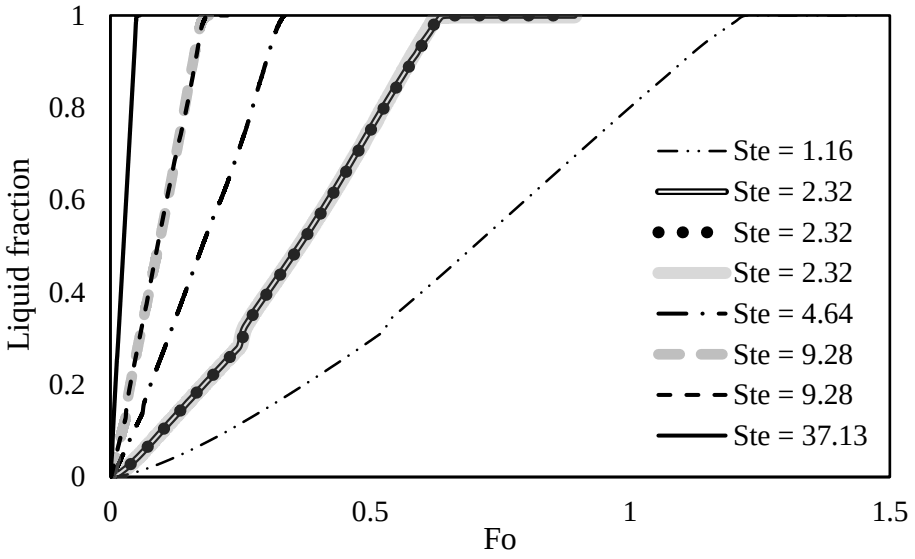

a)

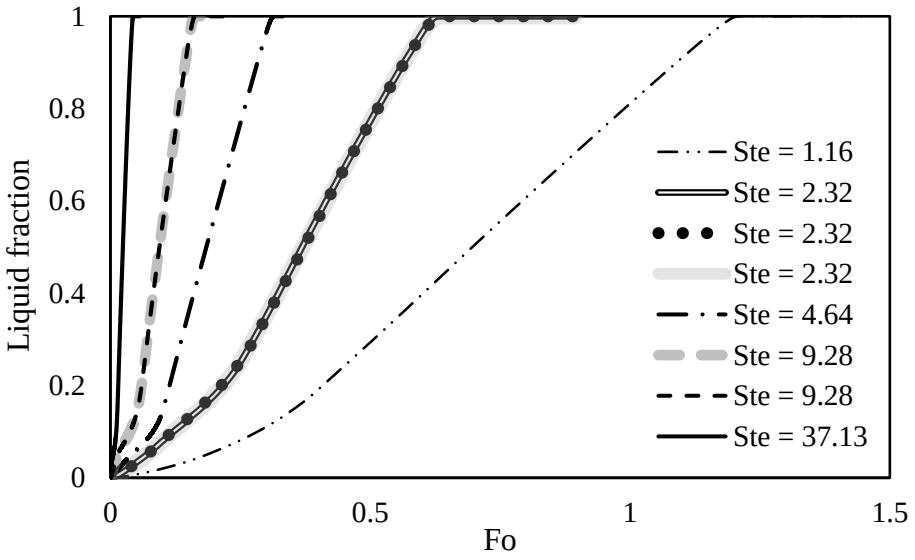

b)

Fig. 20. The variation of Liquid fraction as a function of Fourier number for different Stefan number for LHTES system with a) PCM only and b) composite PCM

Therefore, it is proved that the liquid fraction is a function Stefan number. Based on the literature review and also due to the fact that the liquid fraction is changed directly with the inverse of latent heat of fusion based on the storage capacity of LHTES systems, the liquid fraction is directly a function of Stefan number. The independent parameter of *Fo.Ste* is almost enough for generalization the melting process; however, due to the effect of natural convection especially for high Stefan number cases and especially for the case of PCM only when the effect of natural convection is significant, Rayleigh number is better to be included to propose the effect of natural convection. After careful calculation to find the best combination of *Fo.Ste* with Ra, Figs. 21-a and 21-b display the variation of liquid fraction in terms of $Fo.Ste.Ra^{-0.02}$. For both PCM only and especially composite system, the liquid fractions from all the simulations almost match each others showing a reasonable generalization of the liquid fraction in terms of Fourier, Stefan and Rayleigh number.

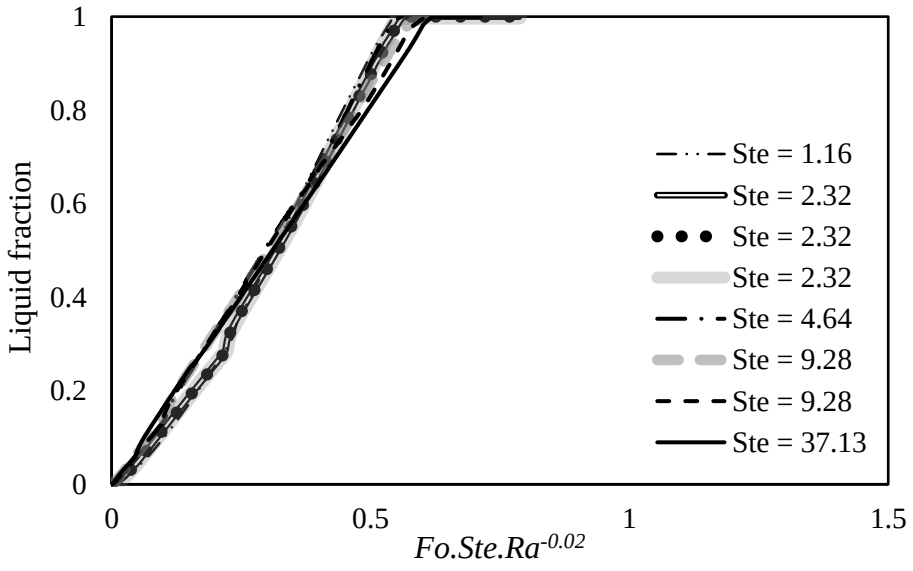

a)

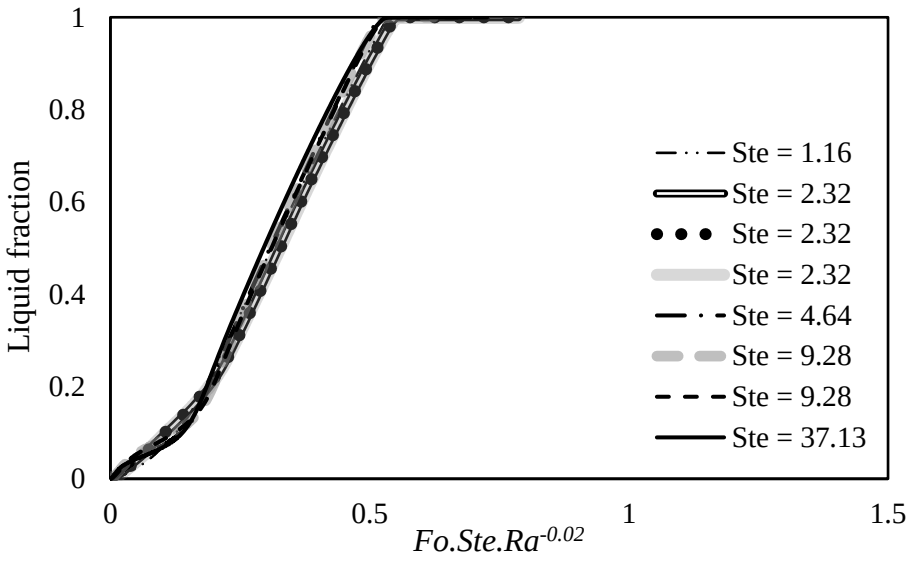

b)

Fig. 21. The variation of liquid fraction in terms of $Fo.Ste.Ra^{-0.02}$ for LHTES system with a) PCM only and b) composite PCM

Since the simulation results correlate well with the proposed non-dimensional number, a curve fitting analysis is performed between liquid fraction and $x=Fo.Ste.Ra^{-0.02}$ for both PCM only and composite PCM systems. The fitted polynomial curves are as follows:

PCM only

$$L_f = = -8.06x^4 + 6.8729x^3 - 0.8998x^2 + 1.5144x - 0.0153 \quad (26\text{-a})$$

Composite PCM

$$L_f = -5.7659x^4 - 1.9444x^3 + 6.1535x^2 - 0.0379x + 0.0172 \quad (26\text{-b})$$

The R-square values for the PCM only and composite PCM correlations are 0.9922 and 0.996, respectively. Note that the fitted equations are reasonable for the rectangular geometry within the parameter range: $1.16< Ste <37.13$, $0< Fo <1.5$, $2.9\times10^4 < Ra < 9.5\times108$, $0< L_f < 1$, $0 < Fo.Ste.Ra^{-0.02} < 0.57$. The maximum deviation of liquid fraction from the curve fitted equations are 0.065 and 0.051, respectively, for the PCM only and composite PCM cases showing the good accuracy of the predicted correlations.

6. Conclusion

Previous research in the area of thermal energy storage with PCM has considered the application to a generic storage system, typically at a large scale for central delivery of thermal energy for industrial and large scale architectural purposes. This work shows that if a PCM storage heater is required in domestic applications, with a unit on the wall of a domestic dwelling, then the surface/volume characteristics and the charging surface position and size are significantly important.

Different dimensions of the thermal storage system show the effect of a high conductivity porous medium in different heat storage system volumes on the melting time, temperature, velocity distributions, and heat transfer rate. After verification of the code, the results showed increase of heat transfer rate by using the porous-PCM storage system. However, the effect depends on the size of the storage unit. Higher effect of porous medium on melting process is observed in the PCM's solid phase zone when the thermal diffusivity increases by almost 2.5 times greater than the PCM only system. Furthermore, the presence of porous medium on the melting time is highly related to the aspect ratio (width and height) of the storage systems. For the PCM only system, the height has a higher effect than the width due to the contribution of natural convection in the free flowing system. Considering equal input heat, by changing the dimensions of the storage system with the same surface area and volume, the melting time reduces by 18.2% in the PCM only case and 7.4% in the porous PCM case by changing the dimensions form 50×100 (W×H) to 200×25 (W×H) showing the decreased effect of the presence of the porous medium on the melting time when the system aspect ratio changes. For the system with the dimensions of 200×100 (W×H), the presence of composite PCM can reduce the melting time up to 17% and 4.5% for heat fluxes of 6.4 kW/m^2 and 1.6 kW/m^2, respectively, over the performance of the PCM only case. The heat flux rate is therefore significant in determining the efficacy of the porous medium's influence on the PCM. The non-dimensional

analysis results in curve fitting correlations between the liquid fraction and $Fo.Ste.Ra^{-0.02}$ for rectangular latent heat storage systems for both PCM only and composite PCM systems within the parameter range of $1.16< Ste <37.13$, $0< Fo <1.5$, $2.9\times10^4 < Ra < 9.5\times108$, $0<L_f < 1$ and $0 < Fo.Ste.Ra^{-0.02} < 0.57$.

7. Acknowledgement

This work was funded by grants from EPSRC (Engineering and Physical Sciences Research Council) from the United Kingdom. The authors would like to acknowledge the financial support.

References

1. Sharma SD, Sagara K. Latent Heat Storage Materials and Systems: A Review. *International Journal of Green Energy*. 2005; 2: 1-56.

2. Shaibani AR, Keshtkar MM, Sardari PT. Thermo-economic analysis of a cold storage system in full and partial modes with two different scenarios: A case study. *Journal of Energy Storage*. 2019; 24: 100783.

3. Zhou D, Zhao CY, Tian Y. Review on thermal energy storage with phase change materials (PCMs) in building applications. *Applied Energy*. 2012; 92: 593-605.

4. Talebizadeh Sardari P, Gidding D, Gillott M, Grant D, Walker G. Effect of Air channel Geometry on the Performance of a Composite Metal Foam-PCM to Air Heat Exchanger. *Innovative Applied Energy (IAPE 2109)*. Oxford, United Kingdom14-15 March 2019.

5. Pereira da Cunha J, Eames P. Thermal energy storage for low and medium temperature applications using phase change materials – A review. *Applied Energy*. 2016; 177: 227-38.

6. Niu F, Ni L, Yao Y, Yu Y, Li H. Performance and thermal charging/discharging features of a phase change material assisted heat pump system in heating mode. *Applied Thermal Engineering*. 2013; 58: 536-41.

7. Esapour M, Hosseini MJ, Ranjbar AA, Pahamli Y, Bahrampoury R. Phase change in multi-tube heat exchangers. *Renewable Energy*. 2016; 85: 1017-25.

8. Esapour M, Hosseini MJ, Ranjbar AA, Bahrampoury R. Numerical study on geometrical specifications and operational parameters of multi-tube heat storage systems. *Applied Thermal Engineering*. 2016; 109: 351-63.

9. Shahsavar A, Shaham A, Talebizadehsardari P. Wavy Channels triple-tube LHS Unit with Sinusoidal Variable Wavelength in Charging/Discharging Mechanism. *International Communications in Heat and Mass Transfer*. 2019; 107: 93-105.

10. Al-Abidi AA, Mat S, Sopian K, Sulaiman MY, Mohammad AT. Internal and external fin heat transfer enhancement technique for latent heat thermal energy storage in triplex tube heat exchangers. *Applied Thermal Engineering*. 2013; 53: 147-56.

11. Wang Y-H, Yang Y-T. Three-dimensional transient cooling simulations of a portable electronic device using PCM (phase change materials) in multi-fin heat sink. *Energy*. 2011; 36: 5214-24.

12. Farid M, Kong WJ. Underfloor heating with latent heat storage. *Proceedings of the Institution of Mechanical Engineers, Part A: Journal of Power and Energy*. 2001; 215: 601-9.

13. Delgado M, Lázaro A, Mazo J, Zalba B. Review on phase change material emulsions and microencapsulated phase change material slurries: Materials, heat transfer studies and applications. *Renewable and Sustainable Energy Reviews*. 2012; 16: 253-73.

14. Jamekhorshid A, Sadrameli SM, Farid M. A review of microencapsulation methods of phase change materials (PCMs) as a thermal energy storage (TES) medium. *Renewable and Sustainable Energy Reviews*. 2014; 31: 531-42.

15. Sushobhan BR, Kar SP. Thermal Modeling of Melting of Nano based Phase Change Material for Improvement of Thermal Energy Storage. *Energy Procedia*. 2017; 109: 385-92.

16. Cheng W-L, Li W-W, Nian Y-L, Xia W-d. Study of thermal conductive enhancement mechanism and selection criteria of carbon-additive for composite phase change materials. *International Journal of Heat and Mass Transfer*. 2018; 116: 507-11.

17. Shahsavar A, Talebizadeh Sardari P, Toghraie D. Free convection heat transfer and entropy generation analysis of water-Fe3O4/CNT hybrid nanofluid in a concentric annulus. *International Journal of Numerical Methods for Heat & Fluid Flow*. 2019; 29: 915-34.

18. Shahsavar A, Godini A, Sardari PT, Toghraie D, Salehipour H. Impact of variable fluid properties on forced convection of Fe 3 O 4/CNT/water hybrid nanofluid in a double-pipe mini-channel heat exchanger. *Journal of Thermal Analysis and Calorimetry*. 2019.

19. Oya T, Nomura T, Okinaka N, Akiyama T. Phase change composite based on porous nickel and erythritol. *Applied Thermal Engineering*. 2012; 40: 373-7.

20. Nomura T, Okinaka N, Akiyama T. Impregnation of porous material with phase change material for thermal energy storage. *Materials Chemistry and Physics*. 2009; 115: 846-50.

21. Sarı A, Karaipekli A. Thermal conductivity and latent heat thermal energy storage characteristics of paraffin/expanded graphite composite as phase change material. *Applied Thermal Engineering*. 2007; 27: 1271-7.

22. Esapour M, Hamzehnezhad A, Darzi AAR, Jourabian M. Melting and solidification of PCM embedded in porous metal foam in horizontal multi-tube heat storage system. *Energy Conversion and Management*. 2018; 171: 398-410.

23. Py X, Olives R, Mauran S. Paraffin/porous-graphite-matrix composite as a high and constant power thermal storage material. *International Journal of Heat and Mass Transfer*. 2001; 44: 2727-37.

24. Mesalhy O, Lafdi K, Elgafy A, Bowman K. Numerical study for enhancing the thermal conductivity of phase change material (PCM) storage using high thermal conductivity porous matrix. *Energy Conversion and Management*. 2005; 46: 847-67.

25. Zhao CY, Lu W, Tian Y. Heat transfer enhancement for thermal energy storage using metal foams embedded within phase change materials (PCMs). *Solar Energy*. 2010; 84: 1402-12.

26. Tian Y, Zhao CY. A numerical investigation of heat transfer in phase change materials (PCMs) embedded in porous metals. *Energy*. 2011; 36: 5539-46.

27. Tay NHS, Bruno F, Belusko M. Experimental validation of a CFD model for tubes in a phase change thermal energy storage system. *International Journal of Heat and Mass Transfer*. 2012; 55: 574-85.

28. Liu Z, Yao Y, Wu H. Numerical modeling for solid–liquid phase change phenomena in porous media: Shell-and-tube type latent heat thermal energy storage. *Applied Energy*. 2013; 112: 1222-32.

29. Sciacovelli A, Colella F, Verda V. Melting of PCM in a thermal energy storage unit: Numerical investigation and effect of nanoparticle enhancement. *International Journal of Energy Research*. 2013; 37: 1610-23.

30. Gupta A, Mathie R, Markides C. An experimental and computational investigation of a thermal storage system based on a phase change material: Heat transfer and performance characterization. *Computational Thermal Sciences: An International Journal*. 2014; 6: 341-59.

31. Hossain R, Mahmud S, Dutta A, Pop I. Energy storage system based on nanoparticle-enhanced phase change material inside porous medium. *International Journal of Thermal Sciences*. 2015; 91: 49-58.

32. Zhang P, Xiao X, Meng ZN, Li M. Heat transfer characteristics of a molten-salt thermal energy storage unit with and without heat transfer enhancement. *Applied Energy*. 2015; 137: 758-72.

33. Mahdi JM, Nsofor EC. Melting enhancement in triplex-tube latent heat energy storage system using nanoparticles-metal foam combination. *Applied Energy*. 2017; 191: 22-34.

34. Al-abidi AA, Bin Mat S, Sopian K, Sulaiman MY, Mohammed AT. CFD applications for latent heat thermal energy storage: a review. *Renewable and Sustainable Energy Reviews*. 2013; 20: 353-63.

35. Nield DA, Bejan A. *Convection in Porous Media*: Springer International Publishing, 2017.

36. Nayak KC, Saha SK, Srinivasan K, Dutta P. A numerical model for heat sinks with phase change materials and thermal conductivity enhancers. *International Journal of Heat and Mass Transfer*. 2006; 49: 1833-44.

37. Vafai K, Tien CL. Boundary and inertia effects on convective mass transfer in porous media. *International Journal of Heat and Mass Transfer*. 1982; 25: 1183-90.

38. Cheng P, Hsu C-T. HEAT CONDUCTION. In: Ingham DB, Pop I, (eds.). *Transport Phenomena in Porous Media*. Oxford: Pergamon, 1998, p. 57-76.

39. Mat S, Al-Abidi AA, Sopian K, Sulaiman MY, Mohammad AT. Enhance heat transfer for PCM melting in triplex tube with internal–external fins. *Energy Conversion and Management*. 2013; 74: 223-36.

40. Li S, Chen Y, Sun Z. Numerical Simulation and Optimization of the Melting Process of Phase Change Material inside Horizontal Annulus. *Energies*. 2017; 10: 1249.

41. Ye W-B, Zhu D-S, Wang N. Numerical simulation on phase-change thermal storage/release in a plate-fin unit. *Applied Thermal Engineering*. 2011; 31: 3871-84.

42. Assis E, Katsman L, Ziskind G, Letan R. Numerical and experimental study of melting in a spherical shell. *International Journal of Heat and Mass Transfer*. 2007; 50: 1790-804.

43. Shahsavar A, Al-Rashed AA, Entezari S, Sardari PT. Melting and Solidification Characteristics of a Double-Pipe Latent Heat Storage System with Sinusoidal Wavy Channels Embedded in a Porous Medium. *Energy*. 2019; 171: 751-69.

44. Xu Y, Ren Q, Zheng Z-J, He Y-L. Evaluation and optimization of melting performance for a latent heat thermal energy storage unit partially filled with porous media. *Applied Energy*. 2017; 193: 84-95.

45. Calmidi VV, Mahajan RL. The Effective Thermal Conductivity of High Porosity Fibrous Metal Foams. *Journal of Heat Transfer*. 1999; 121: 466-71.

46. Xu HJ, Xing ZB, Wang FQ, Cheng ZM. Review on heat conduction, heat convection, thermal radiation and phase change heat transfer of nanofluids in porous media: Fundamentals and applications. *Chemical Engineering Science*. 2019; 195: 462-83.

47. Yang H, Zhao M, Gu ZL, Jin LW, Chai JC. A further discussion on the effective thermal conductivity of metal foam: An improved model. *International Journal of Heat and Mass Transfer*. 2015; 86: 207-11.

48. Boomsma K, Poulikakos D. On the effective thermal conductivity of a three-dimensionally structured fluid-saturated metal foam. *International Journal of Heat and Mass Transfer*. 2001; 44: 827-36.

49. Dai Z, Nawaz K, Park YG, Bock J, Jacobi AM. Correcting and extending the Boomsma–Poulikakos effective thermal conductivity model for three-dimensional, fluid-saturated metal foams. *International Communications in Heat and Mass Transfer*. 2010; 37: 575-80.

50. Bhattacharya A, Calmidi VV, Mahajan RL. Thermophysical properties of high porosity metal foams. *International Journal of Heat and Mass Transfer*. 2002; 45: 1017-31.

51. Boomsma K, Poulikakos D. Corrigendum for the paper: K. Boomsma, D. Poulikakos, "On the effective thermal conductivity of a three-dimensionally structured fluid-saturated metal foam" [International Journal of Heat and Mass Transfer, 44 (2001) 827–836]. *International Journal of Heat and Mass Transfer*. 2011; 54: 746-8.

52. Haussener S, Coray P, Lipiński W, Wyss P, Steinfeld A. Tomography-Based Heat and Mass Transfer Characterization of Reticulate Porous Ceramics for High-Temperature Processing. *Journal of Heat Transfer*. 2009; 132: 023305--9.

53. Žukauskas A. Heat transfer from tubes in crossflow. *Advances in heat transfer*: Elsevier, 1972, p. 93-160.

54. Kuwahara F, Shirota M, Nakayama A. A numerical study of interfacial convective heat transfer coefficient in two-energy equation model for convection in porous media. *International Journal of Heat and Mass Transfer*. 2001; 44: 1153-9.

55. Hwang JJ, Hwang GJ, Yeh RH, Chao CH. Measurement of Interstitial Convective Heat Transfer and Frictional Drag for Flow Across Metal Foams. *Journal of Heat Transfer*. 2001; 124: 120-9.

56. Churchill SW, Chu HHS. Correlating equations for laminar and turbulent free convection from a vertical plate. *International Journal of Heat and Mass Transfer*. 1975; 18: 1323-9.

57. Kim SY, Kang BH, Kim J-H. Forced convection from aluminum foam materials in an asymmetrically heated channel. *International Journal of Heat and Mass Transfer*. 2001; 44: 1451-4.

58. Darzi AR, Farhadi M, Sedighi K. Numerical study of melting inside concentric and eccentric horizontal annulus. *Applied Mathematical Modelling*. 2012; 36: 4080-6.

59. Zhou D, Zhao CY. Experimental investigations on heat transfer in phase change materials (PCMs) embedded in porous materials. *Applied Thermal Engineering*. 2011; 31: 970-7.

60. Pal D, Joshi YK. Melting in a side heated tall enclosure by a uniformly dissipating heat source. *International Journal of Heat and Mass Transfer*. 2001; 44: 375-87.

61. Xu Y, Li M-J, Zheng Z-J, Xue X-D. Melting performance enhancement of phase change material by a limited amount of metal foam: Configurational optimization and economic assessment. *Applied Energy*. 2018; 212: 868-80.

62. Liu Z, Ma C. Numerical analysis of melting with constant heat flux heating in a thermal energy storage system. *Energy Conversion and Management*. 2002; 43: 2521-38.

63. Shatikian V, Ziskind G, Letan R. Numerical investigation of a PCM-based heat sink with internal fins: Constant heat flux. *International Journal of Heat and Mass Transfer*. 2008; 51: 1488-93.

64. Wang P, Wang X, Huang Y, Li C, Peng Z, Ding Y. Thermal energy charging behaviour of a heat exchange device with a zigzag plate configuration containing multi-phase-change-materials (m-PCMs). *Applied Energy*. 2015; 142: 328-36.